

# Investigation of global particulate nitrate from the AeroCom Phase III experiment

Huisheng Bian<sup>1,2</sup>, Mian Chin<sup>2</sup>, Didier A. Hauglustaine<sup>3</sup>, Michael Schulz<sup>4</sup>, Gunnar Myhre<sup>5,6</sup>,  
Susanne E. Bauer<sup>7,8</sup>, Marianne T. Lund<sup>6</sup>, Vlassis A. Karydis<sup>9</sup>, Tom L. Kucsera<sup>10</sup>, Xiaohua Pan<sup>11</sup>,  
Andrea Pozzer<sup>9</sup>, Ragnhild B. Skeie<sup>6</sup>, Stephen D. Steenrod<sup>10</sup>, Kengo Sudo<sup>12</sup>, Kostas  
Tsigaridis<sup>7,8</sup>, Alexandra P. Tsimpidi<sup>9</sup>, and Svetlana G. Tsyro<sup>4</sup>

<sup>1</sup> Joint Center for Environmental Technology UMBC, Baltimore, MD, USA

<sup>2</sup> Laboratory for Atmospheres, NASA Goddard Space Flight Center, Greenbelt, MD, USA

<sup>3</sup> Laboratoire des Sciences du Climat et de l'Environnement (LSCE), UMR8212, CEA-CNRS-UVSQ, Gif-sur-Yvette, France

<sup>4</sup> Norwegian Meteorological Institute, Blindern, Norway

<sup>5</sup> Department of Geosciences, University of Oslo, Oslo, Norway

<sup>6</sup> Center for International Climate and Environmental Research-Oslo, Oslo, Norway

<sup>7</sup> The Earth Institute, Center for Climate Systems Research, Columbia University, New York, USA

<sup>8</sup> NASA Goddard Institute for Space Studies, New York, USA

<sup>9</sup> Max Planck Institute for Chemistry, 55128 Mainz, Germany

<sup>10</sup> Universities Space Research Association, GESTAR, Columbia, MD, USA

<sup>11</sup> School of Computer, Mathematical and Natural Sciences, Morgan State University, Baltimore, MD, USA

<sup>12</sup> Center for Climate System Research, University of Tokyo, Tokyo, Japan.

## Abstract

An assessment of global particulate nitrate and ammonium aerosol based on simulations from nine models participating in the AeroCom Phase III study is presented. A budget analyses was conducted to understand the typical magnitude, distribution, and diversity of the aerosols and their precursors among the models. To gain confidence on model performance, the model results were evaluated with various observations globally, including ground station measurements over North America, Europe, and East Asia for tracer concentrations and dry and wet depositions, as well as with aircraft measurements in the Northern Hemisphere mid-high latitudes for tracer vertical distributions. Given the unique chemical and physical features of the nitrate occurrence, we further investigated the similarity and differentiation among the models by examining: 1) the pH-dependent  $\text{NH}_3$  wet deposition; 2) the nitrate formation via heterogeneous chemistry on the surface of dust and sea-salt particles or thermodynamic equilibrium calculation including dust and sea salt ions; and 3) the nitrate coarse mode fraction (i.e., coarse/total). It is found that  $\text{HNO}_3$ , which is simulated explicitly based on full  $\text{O}_3$ - $\text{HO}_x$ - $\text{NO}_x$ -aerosol chemistry by all models, differs by up to a factor of 9 among the models in its global tropospheric burden. This partially contributes to a large difference in  $\text{NO}_3^-$ , whose atmospheric burden differs by up to a factor of 13. The atmospheric burdens of  $\text{NH}_3$  and  $\text{NH}_4^+$  differ by 17 and 4, respectively. Analyses at the process level show that the large diversity in atmospheric burdens of  $\text{NO}_3^-$ ,  $\text{NH}_3$ , and  $\text{NH}_4^+$  is also related to deposition processes. Wet deposition seems to be the dominant process in determining the diversity in  $\text{NH}_3$  and  $\text{NH}_4^+$  lifetimes. It is critical to correctly account for contributions of heterogeneous chemical production of nitrate on dust and sea-salt, because this process overwhelmingly controls atmospheric nitrate production (typically >80%) and determines the coarse and fine mode distribution of nitrate aerosol.

## 1. Introduction

49 Atmospheric aerosols adversely affect human health and play an important role in  
50 changing the Earth's climate. A series of multimodel studies have been coordinated by  
51 the international activity of Aerosol Comparisons between Observations and Models  
52 (AeroCom) in its Phase I and II model experiments that have systematically assessed the  
53 presence and influence of almost all major atmospheric anthropogenic and natural  
54 aerosols (such as sulfate, dust, and carbonaceous aerosols) (e.g., Kinne et al., 2006;  
55 Schulz et al., 2006; Textor et al., 2006; Koch et al., 2009; Huneus et al., 2011; Tsigaridis  
56 et al., 2014; Kim et al., 2015). Very little attention has been drawn to nitrate aerosol  
57 (hereafter "nitrate" referring to particulate nitrate unless otherwise specified) other than  
58 its contribution to radiative forcing (Myhre et al., 2013). One obvious reason is that not  
59 many models used to include nitrate owing to the chemical complexity of nitrate  
60 formation. However, atmospheric nitrate aerosol not only exerts direct effects on air  
61 quality and climate, but also uniquely impacts the Earth system by being directly  
62 involved in tropospheric chemistry and constraining net primary productivity, hence  
63 altering carbon sequestration and ecological effects, via its deposition (Prentice et al.,  
64 2001).

65  
66 Atmospheric nitrate contributes notably to total aerosol mass in the present-day,  
67 especially in urban areas and agriculture regions. Nitrate is about a quarter of sulfate in  
68 terms of overall global burden, AOD, and direct forcing at the present-day according to  
69 the study of AeroCom II direct forcing experiment (Myhre et al., 2013). This conclusion  
70 is confirmed by recent publications using various individual models and emission  
71 inventories (Bellouin et al; 2011; Bauer et al., 2007; Hauglustaine 2014; Karydis et al.,  
72 2016; Mezuman et al., 2016; Paulot et al., 2016). Regionally, considerable evidences  
73 from in-situ measurements (Bessagnet et al., 2014; Haywood et al., 2008; Jimenez et al.,  
74 2009; Malm et al., 1994; Vieno et al., 2016) and model results (Karydis et al., 2011;  
75 Ensberg et al., 2013; Trump et al., 2015) indicate that nitrate becomes one of the major  
76 aerosol species in urban and agriculture environments. For example, nitrate concentration  
77 is about half of sulfate during the summer season in Beijing (Zhou et al., 2016) and  
78 represents a large portion of wintertime aerosol mass in the San Joaquin Valley in  
79 California (Pusede et al., 2016).

80  
81 More importantly, the relative importance of aerosol nitrate is likely to increase over the  
82 century with a projected decline in SO<sub>2</sub> and NO<sub>x</sub> emissions and increase in NH<sub>3</sub>  
83 emissions (IPCC, 2013). With the reduction of SO<sub>2</sub> emissions, less atmospheric NH<sub>3</sub> is  
84 required to neutralize the strong acid H<sub>2</sub>SO<sub>4</sub>. The excess of NH<sub>3</sub> results in gaseous HNO<sub>3</sub>  
85 and NH<sub>3</sub> entering the condensed phase, and their subsequent dissociation yields nitrate  
86 and ammonium ions. The trend of future nitrate depends on which is the limited species,  
87 NO<sub>x</sub> or NH<sub>3</sub>, for nitrate formation (Tsimplidi et al., 2007; 2008). Generally, our  
88 atmosphere, at its current and foreseeable near future, is still in an NH<sub>3</sub>-limited condition  
89 according to sensitivity studies by Heald et al. (2012) and Walker et al. (2012). Almost  
90 all global models predicted an overall increase of atmospheric nitrate burden during this  
91 century based on current available emission inventories (Bauer et al 2007; 2016; Bellouin  
92 et al., 2011; Hauglustaine et al., 2014; Li et al., 2014). For example, using CMIP5 future  
93 emission projections, Bellouin et al. (2011) concluded that, by 2090, nitrate would  
94 become an important aerosol species in Europe and Asia, contributing up to two thirds of

95 the globally averaged anthropogenic optical depth. However, the predicted trend of  
96 surface nitrate is mixed. Some studies estimated a consistent increase of surface nitrate  
97 (Bellouin et al., 2011), while others pointed out that this increase might vanish or even  
98 reverse over some regional urban areas due to the decline of NO<sub>x</sub> emissions (Bauer et al.,  
99 2016; Pusede et al., 2016; Trail et al., 2014). Nevertheless, the potentially increasing  
100 importance of nitrate in climate and its large uncertainty in future surface nitrate  
101 predictions urge us to characterize model performance and understand the  
102 physicochemical mechanisms behind the diversity of nitrate simulations.

103  
104 Nitrate is also important in that its formation directly affects tropospheric chemistry.  
105 First, the formation of particulate nitrate, through either aqueous phase chemical reaction  
106 between HNO<sub>3</sub> and NH<sub>3</sub> (Metzger et al., 2002; Kim et al., 1993) or heterogeneous  
107 reaction of nitrogen species such as HNO<sub>3</sub>, NO<sub>3</sub>, and N<sub>2</sub>O<sub>5</sub> on the surface of dust and sea  
108 salt aerosol particles (Bauer et al., 2004; 2005; Bian et al., 2003; Dentener 1996; Liao et  
109 al., 2003), converts gas phase nitrogen species into aerosols. Consequently, the global  
110 tropospheric NO<sub>x</sub> concentration and the rate of conversion of N<sub>2</sub>O<sub>5</sub> to HNO<sub>3</sub> will be  
111 reduced (Riemer et al., 2003), which in turn leads to the reduction of atmospheric  
112 oxidants. For example, global tropospheric O<sub>3</sub> can be reduced by 5% (Bauer et al., 2007)  
113 and tropical Atlantic OH by 10% (Bian et al., 2003) just through the heterogeneous  
114 reactions of nitrogen radicals on dust. Second, the most important removal path for  
115 nitrogen from the atmosphere is the formation of HNO<sub>3</sub>, which is subsequently deposited  
116 (Riemer et al., 2003). Since HNO<sub>3</sub> is subject to partitioning between the gas and aerosol  
117 phases, the lifetimes of nitrogen species can be shortened by the formation of  
118 tropospheric nitrate aerosol because the loss of total HNO<sub>3</sub> will be accelerated by a much  
119 higher dry deposition in the aerosol phase.

120  
121 Large nitrogen deposition occurs over both land and ocean (Dentener et al., 2006;  
122 Kanakidou et al., 2012; 2016). Nitrogen deposition can either benefit or impair ecosystem  
123 productivity depending on the initial balance of nutrients since different ecosystems have  
124 different Nr (reactive nitrogen including gas and particulate NO<sub>3</sub><sup>-</sup> and other nitrogen  
125 compounds) availability and retention (Galloway et al., 2004; Prentice et al., 2001). If  
126 fixed Nr is deposited as nitrate in forests, it may act as a "fertilizer," stimulating growth  
127 and thus enhancing carbon sequestration (Fowler et al., 2015). But when the accumulated  
128 deposition exceeds the nutritional needs of the ecosystem, nitrogen saturation may result  
129 (Fenn et al., 1996). Soil fertility declines due to the leeching of cations (Milegroet and  
130 Cole, 1984) and, thus, carbon uptake diminishes. The balance between fertilization and  
131 saturation depends on the spatial and temporal extent of nitrogen deposition. In order to  
132 determine the extent to which the emissions of air pollutants will have to be reduced and  
133 whether the environment needs to be protected from damage, it is essential to know  
134 where and by how much N deposition exceeds nature's tolerance (Dentener et al. 2006;  
135 Lamarque et al., 2005; Phoenix et al., 2006).

136  
137 Here we present a nitrate-focused study that has been organized as a part of the series of  
138 AeroCom phase III experiments (<https://wiki.met.no/aerocom/phase3-experiments>). The  
139 goals of this activity are to (1) address the diversity of the nitrate simulation by the  
140 AeroCom multi-models and diagnose the driving processes for the diversity, (2) explore

141 the uncertainty of the model nitrate simulations constrained against various  
142 measurements from ground station networks and aircraft campaigns, and (3) investigate  
143 how the formation of nitrate changes in different models in response to perturbation on  
144 key precursors and factors that determine nitrate formation. We focus on the first two  
145 objectives in this paper. Such a study directs us on how to improve the representation of  
146 nitrate aerosol formation and size distribution in climate chemistry models and reveals  
147 nitrate effects on global air quality and climate.

148

149 Building upon the analysis of the multi-model diversity, three additional sensitivity  
150 experiments are designed using the GMI model to further explore the potential sources  
151 for the diversity on physical and chemical process-level. First, we explore the impact of  
152 pH-dependent  $\text{NH}_3$  wet deposition on atmospheric  $\text{NH}_3$  and associated nitrogen species.  
153 We then reveal the importance of mineral dust and sea salt in the nitrate formation and  
154 check the resultant nitrate aerosol size distribution that is particularly important in nitrate  
155 forcing estimation.

156

157 The paper is organized as follows. Section 2 introduces the experiment setup including  
158 the emission inventories used and the participating AeroCom models. Observations of  
159 surface tracer concentrations and dry and wet depositions over U.S., Europe, and East  
160 Asia, as well as aircraft measurements in the ARCTAS campaigns are described in  
161 section 3. We present AeroCom model inter-comparison and the model evaluation using  
162 aforementioned observations in section 4. Based on the knowledge from previous  
163 sections, we further discuss nitrate formation in response to physiochemical  
164 methodologies in section 5 and summarize our major findings in section 6.

165

## 166 **2. Experiment setup and AeroCom model description**

167

### 168 **2.1 Experiment setup**

169 The AeroCom III nitrate experiment comprises one baseline and six perturbation  
170 simulations, with the latter designed for assessing the possible future changes of emission  
171 and meteorological fields relevant to nitrate formation. Models are advised to use the  
172 same prescribed emission datasets for gases and aerosols. Emissions from anthropogenic,  
173 aircraft, and ship for aerosol and ozone simulations are obtained from the recently  
174 developed HTAP v2 database (Janssens-Maenhout et al., 2015) that provides high spatial  
175 resolution monthly emission. For the tracers that are included in ozone chemistry but are  
176 not provided by HTAP v2 (i.e. some volatile organic compounds), they should be  
177 obtained from CMIP5 RCP85 with a linear interpolation between 2005 and 2010.

178 Biomass burning emissions are the emissions of GFED3 (Werf et al., 2010) in 2008

179 [<http://www.globalfiredata.org/data.html>]. The  $\text{NH}_3$  emission from ocean is adopted  
180 based on the compilation of GEIA emission inventory [Bouwman et al., 1997].

181 Participating modeling groups use their own emissions of dimethyl sulfide (DMS), dust,  
182 sea salt, and NO from lightning, since they are calculated based on models'  
183 meteorological fields.

184

185 A full year simulation for 2008 is required for the nitrate model experiment. There are  
186 several in-situ observation datasets available in 2008 for model evaluation, including the

187 surface concentration and deposition measurements over the US (CastNet, AMoN,  
188 NDAP/NTN), Europe (EMEP), and Asia (EANET), and the aircraft measurements of  
189 vertical profiles (e.g. ARCTAS-A, ARCTAS-CARB, and ARCTAS-B). All participating  
190 models are required to use the reanalysis or nudged meteorological data for 2008 and  
191 allow one-year spin up for the baseline simulation.

192

## 193 **2.2 AeroCom models**

194 Nine models participate in the AeroCom III nitrate experiment. Their general nitrate-  
195 related physiochemical mechanisms are summarized in Table 1. Further detailed  
196 information on their thermodynamic equilibrium model (TEQM) is given in Table 2.

197

198 The models participating in this study are divided into two groups. Group one (CHASER,  
199 EMAC, INCA, GISS-MATRIX, and GISS-OMA) run chemical fields together with  
200 meteorological fields, while group two (EMEP, GMI, OsloCTM2, and OsloCTM3)  
201 simulate chemical fields using archived meteorological fields. Most models in this study  
202 have a horizontal resolution around 2-3 degrees except EMEP with 0.5 degree.

203 Vertically, most models cover both the troposphere and the stratosphere with a peak  
204 altitude up to 0.01 hPa except EMEP that extends vertically up to 100 hPa into the  
205 troposphere only.

206

207 All models use full gas phase  $O_3$ - $NO_x$ - $HO_x$  chemistry to produce  $HNO_3$  and consider the  
208 feedback of nitrate aerosol formation on  $HNO_3$  calculation (i.e. changes in  $HNO_3$   
209 concentrations due to the gas/particle equilibrium). Meanwhile, all models consider  $N_2O_5$   
210 hydrolysis, the conversion of  $N_2O_5$  to  $HNO_3$ . The first order loss reaction occurs on the  
211 surface of tropospheric aerosols and assumes irreversible instant reaction. However, the  
212 models differ in  $N_2O_5$  hydrolysis by considering the reaction on the surface of different  
213 aerosol types. Uptake coefficients (aka gamma factors) also differ in their relationship to  
214 temperature and RH. CHASER model is special as it allows  $N_2O_5$  conversion to  $HNO_3$   
215 on liquid cloud particles. Please refer to Table 1 and the listed references for details. Due  
216 to the complexity of chemical mechanisms for organic nitrate compounds and different  
217 recommendations for reaction rates,  $HNO_3$  fields produced by the models differ greatly.  
218 This difference propagates into the subsequent gas-aerosol reactions for nitrate formation.

219

220 These models are very different in their approaches on gas-aerosol reactions in nitrate  
221 formation. All models consider reactions between  $NH_3$  and  $HNO_3$ . However, models  
222 differ dramatically in whether to include contributions of dust and sea salt (Table 1).  
223 Some account for both, some for only dust or sea salt, and some do not account for any of  
224 them at all. The methods used by the models in accounting for  $NH_3$  and dust/sea salt  
225 contributions are also different. Please also note that the heterogeneous chemical  
226 production of particulate nitrate mentioned in this paper refers only to the first order loss  
227 reaction of  $HNO_3$  on the surface of dust and sea salt particles. A series of reactions, such  
228 as  $N_2O_5$  hydrolysis and  $BrONO_2$  hydrolysis, affect  $HNO_3$  simulation. These reactions are  
229 typically considered in  $O_3$ - $NO_x$ - $HO_x$  chemistry and their discussion is beyond the scope  
230 of this paper.

231

232 All participating models adopt TEQM to deal with aqueous and solid phase reactions and  
233 gas-aerosol partitioning (Tables 1 and 2). This is based on the assumption that volatile  
234 species in the gas and aerosol phases are generally in chemical equilibrium. However, the  
235 assumption is not always warranted in some cases, as we will discuss in section 5.2. Even  
236 with the TEQM approach, nitrate calculation could differ due to treatments of  
237 equilibrium constants or chemical potentials, solute activity coefficients, water activity,  
238 and relative humidity of deliquescence (RHD). The parameterizations adopted by the  
239 models to deal with multicomponent activity coefficient, binary activity coefficient, and  
240 water activity are given in table 2. GISS-OMA, Oslo-CTM2 and Oslo-CTM3 are special  
241 in that they assume aerosols to be metastable so that the model does not take into account  
242 formation of solids in this study. All other models do consider the effect of the hysteresis  
243 of particle phase transitions. All models also assume that the overall particles are large  
244 enough to neglect the Kelvin effect.

245  
246 The participating models call the TEQMs in different ways to account for aerosol size  
247 effect. All the TEQMs (ISORROPIA-I, ISORROPIA-II, MARS, RPMIRES, INCA, and  
248 EQSAM3) assume particles to be internally mixed, i.e. all particles of the same size have  
249 the same composition. However, some parent models (CHASER, EMEP, GMI, INCA,  
250 GISS-MATRIX and GISS-OMA) call their TEQMs only once for fine mode aerosol  
251 particles, while the others (EMAC, OsloCTM2 and OsloCTM3) call their TEQMs from  
252 different aerosol size bins. For example, Oslo-CTM2 and Oslo-CTM3 consider a bi-  
253 modal aerosol size-spectrum with two major aerosol modes, fine and coarse, and  
254 calculate gas-aerosol equilibrium partitioning with EQSAM3 first for fine mode and then  
255 for coarse mode. Additionally, to account for kinetic limitations, EMAC calculates the  
256 phase partitioning in two stages. In the first stage, the amount of the gas-phase species  
257 that is able to kinetically condense onto the aerosol phase within the model time step is  
258 calculated, while in the second stage, the TEQM redistributes the mass between the two  
259 phases assuming instant equilibrium (Pringle et al., 2010).

260  
261 The TEQMs also differ in the chemical components considered. Specifically, the TEQMs  
262 in CHASE, EMEP, GISS-MATRIX, GISS-OMA, GMI and INCA include only species  
263 of sulfate, nitrate, ammonium and their gas, liquid, and solid components. The models  
264 Oslo-CTM2 and Oslo-CTM3 add NaCl and HCl, while the model EMAC further expands  
265 the species by including dust-related crustal material such as  $\text{Ca}^{2+}$ ,  $\text{K}^{+}$ , and  $\text{Mg}^{2+}$ .

266  
267 These TEQMs differ in their computational approaches as well. Computational efficiency  
268 is a prime consideration for a TEQM that is designed for incorporation into a global air  
269 quality and climate study. To speed up the calculation, TEQMs typically divide the  
270 system into sub-domains based on RH and concentrations of ammonium, sodium, crustal  
271 cations, and sulfate. Corresponding approximation could be adopted for each sub-domain  
272 with the minimum numbers of equilibriums and unknown components. As listed in table  
273 2, the numbers of sub-domains are 4, 5, 4, 2, 3, and 3 for the TEQM ISORROPIA-I,  
274 ISORROPIA-II, MARS, RPMIRES, INCA, and EQSAM3, respectively.

275  
276 The ways to account for the contribution of dust and sea salt to nitrate formation are also  
277 different (see Table 1 column “How do CHEMDUSS”). Some models (EMAC, Oslo-

278 CTM3, and Oslo-CTM2) include dust and/or sea salt components in their TEQM models  
279 directly (marked as TEQM in Table 1 under column “How do CHEMDUSS”), while  
280 some models (EMEP, GISS-OMA, GMI, and INCA) use an approach of first order loss  
281 rate outside their TEQMs to account for the heterogeneous reactions of HNO<sub>3</sub> on the  
282 surface of dust and sea salt (marked as HETCHEM in Table 1). For the latter approach,  
283 the gamma rates and their RH dependence adopted by the models differ as well.

284

285 Dry and wet deposition of NH<sub>3</sub>, ammonium nitrate, and ammonium sulfate are treated  
286 similarly to other gas and aerosol tracers in the models. It is worth pointing out that there  
287 is a different consideration for Henry’s law constant of NH<sub>3</sub> used by the models. Some  
288 models modify it based on the pH value of cloud water while others do not. We will  
289 discuss the impact of these two treatments on nitrate simulation in section 5.1.

290

291 We introduce only the major characteristics of thermodynamic equilibrium models since  
292 this study aims for the evaluation and explanation of overall nitrate diversity among the  
293 GCM/CTM models from all potential aspects. The detailed discussion of the models  
294 chemical mechanism of gas phase reactions and the aerosol optical properties adopted by  
295 the models is also beyond this work. Readers could refer to the references listed in Tables  
296 1 and 2 for any further details.

297

### 298 **3. Observations**

299 We use surface measurements from ground station networks and aircraft campaigns to  
300 evaluate modeled surface concentrations, dry and wet depositions, and vertical  
301 distributions of nitrate and related species (Table 3).

302

#### 303 **3.1 Surface measurements of concentrations and deposition rates**

304 Ambient concentrations of sulfur and nitrogen species throughout the US and Canada  
305 have been measured by the ground station network CASTNET (Clean Air Status and  
306 Trends Network) (Figure 1). The measurements use a 3-stage filter pack with a controlled  
307 flow rate. The measurements of CASTNET do not include NH<sub>3</sub>. AMoN (Ammonia  
308 Monitoring Network), measuring concentrations of ambient NH<sub>3</sub>, has been deployed at  
309 CASTNET sites starting from October 2007 using passive samplers. The corresponding  
310 tracers’ surface concentration measurements over Europe have been conducted by EMEP  
311 (The European Monitoring and Evaluation Programme). The measured sites of all these  
312 networks are located in rural areas or sensitive ecosystems, representing a larger region  
313 by avoiding influences and contamination from local sources. Surface concentrations  
314 over East Asia are inferred from the measurement of dry deposition by EANET (Acid  
315 Deposition Monitoring Network in East Asia). This network provides acid deposition  
316 from a regional monitoring network including 13 countries in East Asia using  
317 standardized monitoring methods and analytical techniques.

318

319 CASTNET also provides dry deposition of sulfate and nitrogen species. Direct  
320 measurements of dry deposition fluxes (D) are expensive so D is calculated as the  
321 measured pollutant concentration (C) multiplied by the modeled dry deposition velocity  
322 ( $V_d$ ).  $V_d$  is either estimated by the Multi-Layer Model fed with measured hourly

323 meteorological data or derived from historical average  $V_d$  for sites with discontinued  
324 meteorological parameters.

325  
326 Direct measurements of wet deposition fluxes of sulfate, nitrate, and other ions have also  
327 been performed by NADP/NTN (the National Atmospheric Deposition Program /  
328 National Trends Network) across the contiguous US, Canada, Alaska, and the US Virgin  
329 Islands and EANET over East Asia. Sites are predominantly located away from urban  
330 areas and point sources of pollution. Each site has a precipitation chemistry collector and  
331 gauge. Both networks can measure wet deposition for a continuous period (weekly for  
332 NADP/NTN and daily for EANET), or every precipitation event if using an automated  
333 collector (wet-only sampling).

334  
335 Data is quality assured for all measurements. Measurements over North America use  
336 automated screening techniques, semi-annual calibration results, site operator comments,  
337 and manual data review. Quality assurance of EMEP is carried out on both the national  
338 level and by the Chemical Co-ordinating Centre (CCC). The quality of EMEP  
339 measurements is not equal at the national level (Schaap et al., 2002; 2004). Sites in  
340 North, Western and Central Europe were generally well equipped and performing, while  
341 sites in the rest of Europe suffered from inadequate sampling and calibrating methods due  
342 to political and/or economical reasons. The quality of ammonia measurement is relatively  
343 low since some laboratories experienced contamination problems (Williams et al., 1992).  
344 Although EANET adopts standardized monitoring methods and analytical techniques,  
345 quality assurance is carried out on the national level.

### 346 347 **3.2 Aircraft measurements of vertical profiles**

348 Aircraft campaign measurements during the 2008 Arctic Research of the Composition of  
349 the Troposphere from Aircraft and Satellites (ARCTAS) are used to evaluate tracer  
350 vertical distribution simulated by the models (Bian et al., 2013; Jacob et al., 2010). Three  
351 phases of the campaign, ranging from Northern Hemisphere mid-latitude industrial  
352 region (ARCTAS-CARB, June 2008) to high latitude Arctic regions influenced by long-  
353 rang pollution transport (ARCTAS-A, April 2008) and by local boreal biomass burning  
354 (ARCTAS-B, July 2008), provide well encompassing environment observations. All  
355 flights were conducted by the NASA DC-8 aircraft and the flight tracks of these three  
356 phases are presented in Figure 2. An onboard HR-ToF-AMS instrument (Cubison et al.,  
357 2011; DeCarlo et al, 2006) measured fine mode aerosol concentrations (PM<sub>1</sub>) along the  
358 flight track including  $\text{NO}_3^-$ ,  $\text{NH}_4^+$ , and  $\text{SO}_4^{2-}$  at STP conditions (1013mb and 273.15K) at a  
359 sampling time interval of ~12 seconds. Accuracy estimate of 2-standard deviations, likely  
360 conservative, is 34% for inorganics, dominated by the uncertainty in particle collection  
361 efficiency due to particle bouncing (Huffman et al., 2005).

## 362 363 **4. Model intercomparison and evaluation**

### 364 365 **4.1 AeroCom model inter-comparisons of global distributions and budgets**

#### 366 **4.1.1 $\text{NH}_3$ and $\text{NH}_4^+$**

367 Six models use HTAP2 anthropogenic emissions, two (GISS-MATRIX and GISS-OMA)  
368 use CMIP5 emissions, and one (INCA) uses ECLIPSE emissions. Table 4b shows that



369 eight models have the annual  $\text{NH}_3$  emission values within 5% of the value from the  
370 AeroCom experiment recommended emission inventories, but INCA is 11% higher. The  
371 similar emission distributions ensure that the examined inter-model diversities are truly  
372 caused by the differences in physicochemical processes among the models. The  
373 normalized root-mean-square deviation (NRMSD) of  $\text{NH}_3$  global burden among models  
374 is 1.17 and 0.33 with and without EMAC included. This drastic change in global burden  
375 NRMSD by EMAC is caused by its special treatment of wet deposition. In fact, the  
376 removal of trace gases and aerosol particles by clouds and precipitation in EMAC is not  
377 calculated based on empirically determined, fixed scavenging coefficients, but rather by  
378 solving a system of coupled ordinary differential equations, explicitly describing the  
379 processes involved (Tost et al., 2006). This method resolves feedback mechanisms  
380 between the multi-phase chemistry and transport processes involved. The liquid phase  
381 reaction set used converts all the scavenged  $\text{NH}_3$  (or  $\text{HNO}_3$ ) into  $\text{NH}_4^+$  (or  $\text{NO}_3^-$ ) in the  
382 liquid phase so that at the end everything that is deposited is the total  $\text{NH}_4^+$  and  $\text{NH}_3$ .

383

384 Atmospheric  $\text{NH}_4^+$  is produced entirely by  $\text{NH}_3$  chemical transformation. The models  
385 simulate  $\text{NH}_4^+$  much closer in chemical production (difference less than a factor of 2) than  
386 in lifetime (difference up to a factor of 5.2), indicating removing rates are a key factor in  
387 controlling the global burden of  $\text{NH}_4^+$ . For example, CHASER has a much longer lifetime  
388 of  $\text{NH}_4^+$  (i.e. 9.8 days versus 4.3 days in average), which indicates a slow deposition  
389 removal of  $\text{NH}_4^+$  from the atmosphere. Consequently, CHASER simulates a much higher  
390 atmospheric  $\text{NH}_4^+$  burden than other models.

391

#### 392 **4.1.2 $\text{HNO}_3$ and $\text{NO}_3^-$**

393  $\text{HNO}_3$ , an important nitrate precursor, differs by up to a factor of 9 in its global  
394 tropospheric burden among the models (Table 4c). All models simulated  $\text{HNO}_3$  based on  
395 a full gas phase  $\text{O}_3$ - $\text{HO}_x$ - $\text{NO}_x$  chemistry and coupled it with aerosol chemistry. This  
396  $\text{HNO}_3$  diversity will naturally be propagated into the  $\text{NO}_3^-$  simulation. However, further  
397 discussion of the detailed consideration of full gas-aerosol chemistry for  $\text{HNO}_3$  diversity  
398 among the models is beyond the scope of this study.

399

400 The resultant aerosol product (i.e.,  $\text{NO}_3^-$ ) does not entirely follow its precursor (i.e.,  
401  $\text{HNO}_3$ ) in terms of global burden: EMEP has very low  $\text{HNO}_3$  but high  $\text{NO}_3^-$ , two GISS  
402 models (MATRIX and OMA) simulate high  $\text{HNO}_3$  but low  $\text{NO}_3^-$ , while OsloCTM3 has  
403 an average  $\text{HNO}_3$  but more than triple high  $\text{NO}_3^-$  than average (Tables 4a and 4c).  
404 Furthermore, the difference in  $\text{NO}_3^-$  global burden (up to a factor of 13) is larger than that  
405 of  $\text{HNO}_3$ . Differences in chemical mechanisms of  $\text{NO}_3^-$  production could be a potential  
406 explanation along with the difference in  $\text{HNO}_3$  precursor. Unfortunately, only GMI and  
407 INCA provide a detailed  $\text{NO}_3^-$  chemistry budget analysis. Nevertheless, we can infer that  
408 the total chemical production of  $\text{NO}_3^-$  must be very low ( $\sim 10\text{Tg}$ ) in the two GISS models  
409 while very high ( $> 100\text{Tg}$ ) in OsloCTM2 and OsloCTM3 based on the reported total  
410  $\text{NO}_3^-$  loss. Combining this information with the  $\text{HNO}_3$  global tropospheric burden (Table  
411 4c), we can further infer that the chemical conversion from  $\text{HNO}_3$  to  $\text{NO}_3^-$  must be lowest  
412 in the two GISS models while highest in the two Oslo models. Several factors could  
413 influence this conversion, such as the availability of alkaline species of mineral dust and  
414 sea-salt particles and the physicochemical mechanism of nitrate formation on dust and

415 sea-salt, availability of  $\text{NH}_3$  after combining with  $\text{SO}_4^{2-}$ , and the atmospheric  
416 meteorological fields of temperature and relative humidity. More discussions are given in  
417 sections 5.2 and 5.3.

418

419 Atmospheric lifetime of  $\text{NO}_3^-$  differs up to a factor of 4, from about 2 days in GMI and  
420 OsloCTM2 to larger than 7 days in GISS-OMA and GISS-MATRIX. The slower removal  
421 processes in the two GISS models compensate the low chemical production and help to  
422 maintain their  $\text{NO}_3^-$  atmospheric burden (Figure 3 and Table 4a).

423

## 424 **4.2 Model-observation comparisons**

425

### 426 **4.2.1 Comparisons of surface concentrations over North America, Europe, and East** 427 **Asia**

428 Understanding diversity among model simulations and potential physicochemical  
429 processes behind the difference is important but not sufficient. The information has to be  
430 combined with the knowledge of model performance obtained directly from comparisons,  
431 particularly down to processes level, against various measurements to gain a direction of  
432 any improvement. Figures 4a-c show a model-observation comparison for surface  
433 mass/volume mixing ratios of  $\text{NO}_3^-$ ,  $\text{NH}_4^+$ ,  $\text{NH}_3$ ,  $\text{HNO}_3$ , and  $\text{SO}_4^{2-}$  over North America  
434 (CastNET), Europe (EMEP), and East Asia (EANET). Each point represents a monthly  
435 mean concentration at one observational site. Generally, the agreement between model  
436 and observation is better for aerosol components than for gas tracers (i.e. the precursor  
437 species  $\text{NH}_3$  and  $\text{HNO}_3$ ) over all three regions. All models underestimate  $\text{NH}_3$  surface  
438 volume mixing ratio with a ratio of model to observation down to 0.14, while most  
439 models overestimate surface  $\text{HNO}_3$  volume mixing ratio with a ratio up to 3.9 over North  
440 America. The worse performances of  $\text{NH}_3$  against observations may be also associated to  
441 their relatively lower measurement accuracy, i.e. easier to be contaminated during  
442 measurement (Williams et al., 1992). Among aerosol simulations, model performance is  
443 very similar for  $\text{NH}_4^+$  and  $\text{SO}_4^{2-}$ , while slightly worse for  $\text{NO}_3^-$  that is dispersed further  
444 away from the 1:1 line, particularly at low  $\text{NO}_3^-$  values. The  $\text{NO}_3^-$  simulation over East  
445 Asia is worst with the average normalized root mean square to be 1.3 and 1.8 higher than  
446 that over North America and Europe, respectively.

447

### 448 **4.2.2 Comparisons of vertical profiles with aircraft measurements during the** 449 **ARCTAS field campaign**

450 Evaluation of model performance presented in 4.2.1 for the surface concentrations in the  
451 source regions is highly dependent on the accuracy of the emission inventory. On the  
452 other hand, evaluation using aircraft measurements, particularly over remote regions,  
453 provides further examination of models' physicochemical evolution during transport.  
454 Here we use data from three phases of the ARCTAS aircraft campaign (section 3), and  
455 the results are shown in Figure 5. All model results of  $\text{NO}_3^-$ ,  $\text{NH}_4^+$ , and  $\text{SO}_4^{2-}$  are sampled  
456 along flight track and averaged regionally within 1km vertically for each campaign phase  
457 before comparing with the corresponding aircraft measurements. Note that only EMAC,  
458 EMEP and GMI report daily 3D global tracer concentrations, while the others report  
459 monthly only. Note also that only EMEP and GMI adopt daily biomass burning emission  
460 while the others use monthly emission. To verify the representativeness of monthly mean

461 concentration in capturing the main features exhibited in model-observation comparisons,  
462 daily and monthly concentrations of the three models are used in the same spatial  
463 sampling to compare with the measurements (see the green lines for daily and red for  
464 monthly in the figure). The comparison keeps its main features as shown when using both  
465 daily and monthly model data.

466  
467 During ARCTAS-A, which was conducted in April 2008 and was based in Fairbanks,  
468 Alaska, none of the models captures the long-range transport of aerosols primarily from  
469 Asia, which enter Polar Regions at altitudes between 2-7 km (Fig. 3 in Bian et al., 2013).  
470 Except CHASER and EMAC, all models also report a significant underestimation of  
471  $\text{NH}_4^+$  and  $\text{SO}_4^{2-}$  in boundary layer. A previous assessment of pollution transport to the  
472 Arctic indicated that aerosol wet removal plays an important role in the uncertainty of  
473 Arctic aerosols (Shindell et al., 2008). Another potential reason is that some large fire  
474 activities in Siberia during April 2008 (Jacob et al., 2010) may be missed in the GFED3  
475 emission inventory. The underestimation of  $\text{SO}_4^{2-}$  may help bring up  $\text{NO}_3^-$  production,  
476 particularly at high altitudes. During ARCTAS-CARB, which was conducted in June  
477 2008 based in Palmdale, California, agreement between model and measurements is  
478 much improved. Almost all models show a rapid vertical decrease from surface to free  
479 troposphere, which is consistent with the measurements of  $\text{SO}_4^{2-}$  and  $\text{NH}_4^+$ , but not  $\text{NO}_3^-$ .  
480 The observation shows a maximum of  $\text{NO}_3^-$  at about 1.5 km, which is not represented by  
481 any of the models. During ARCTAS-B, which was conducted in July 2008 and was based  
482 in Cold Lake, Canada, when there were frequent local wild fires, model performances are  
483 mixed. In general, most models underestimate concentrations of  $\text{NO}_3^-$ ,  $\text{NH}_4^+$  and  
484  $\text{SO}_4^{2-}$  below 4 km. CHASER model is special in that it overestimates  $\text{SO}_4^{2-}$  significantly.  
485 This may be contributed to high (near surface) to comparable (free troposphere) model  
486 simulation of  $\text{NH}_4^+$  but an underestimation of  $\text{NO}_3^-$ . Different from other models, the  
487 INCA model shows an enhancement of pollutants in the upper troposphere with  
488 concentrations much higher (more than 5 times) than observations. This behavior may be  
489 derived from a much vigorous vertical uplifting to the upper troposphere as revealed from  
490 Fig. 3a-3b combined with a low  $\text{NH}_3$  Henry's law constant used by INCA, see discussion  
491 in section 5.2.

492  
493 Note that all measurements and model data we discussed above are for fine mode  
494 aerosols. Total  $\text{NO}_3^-$  (orange line using monthly model output) is also shown in the figure  
495 to reveal whether a changing of partitioning of fine and coarse mode  $\text{NO}_3^-$  could improve  
496 the model-observation comparison. It seems that the new version of OsloCTM3 may put  
497 too much of  $\text{NO}_3^-$  in coarse mode.

### 498 499 **4.3 Model-observation comparison for dry and wet deposition**

#### 500 501 **4.3.1 Dry deposition**

502 The budget analyses in section 4.1 concluded that dry and/or wet depositions are most  
503 likely the main processes driving the diversity in the model simulations. Thus, further  
504 evaluation of deposition processes is needed to identify any potential problematic model.  
505

506 The dry depositions of  $\text{NO}_3^-$ ,  $\text{NH}_4^+$ ,  $\text{HNO}_3$ , and  $\text{SO}_4^{2-}$  simulated by the models are  
507 compared against CASTNET measurements over North America (Figure 6). Generally,  
508 the overestimation of surface  $\text{HNO}_3$  concentrations (Figure 3a) results in the higher dry  
509 depositions of  $\text{HNO}_3$ , but this is not the case for  $\text{NO}_3^-$ . Meanwhile, most of the models  
510 give a better dry deposition simulation for aerosol  $\text{SO}_4^{2-}$  and  $\text{NH}_4^+$  than for aerosol  $\text{NO}_3^-$ ,  
511 except CHASER. Specifically, GISS-OMA and GISS-MATRIX have wide spread dry  
512  $\text{NO}_3^-$  deposition at any given measurement value. In other words, the two models  
513 underestimate  $\text{NO}_3^-$  dry deposition significantly at many observational stations, which  
514 does not occur in the other models. This low dry deposition simulation may occur outside  
515 North America as well because the global dry depositions of the two models are lower  
516 than others (Table 4a). OsloCTM2 overestimates  $\text{NO}_3^-$  dry deposition significantly, which  
517 is probably linked to its larger coarse fraction of the nitrate aerosol (see discussion in  
518 section 5.3). OsloCTM3 improved its dry deposition scheme although the model still  
519 overestimates the dry deposition. We will discuss the OsloCTM2  $\text{NO}_3^-$  simulation over  
520 North America by combining the model's wet deposition in the next section.  $\text{NH}_4^+$  dry  
521 deposition is low in GMI but very high in CHASER. This performance is also extended  
522 globally as summarized in Table 4b.

523

#### 524 **4.3.2 Wet deposition**

525 The wet deposition simulations from the nine models are compared with surface  
526 measurement over North America (Figure 7a) and East Asia (Figure 7b) for oxidized  
527  $\text{NO}_3^-$  (i.e. total  $\text{NO}_3^-$  and  $\text{HNO}_3$ ), total  $\text{NH}_4^+$  and  $\text{NH}_3$  ( $\text{tNH}_4^+$ ), and  $\text{SO}_4^{2-}$ . All models tend  
528 to underestimate the wet deposition of  $\text{tNH}_4^+$  and  $\text{SO}_4^{2-}$  over the two regions. Models  
529 EMAC, GMI, OsloCTM2 and OsloCTM3 have relatively high wet removal for oxidized  
530  $\text{NO}_3^-$ , while EMEP removes much less than others over North America. All models' wet  
531 deposition of oxidized  $\text{NO}_3^-$  is biased low over East Asia. As we discussed above,  
532 OsloCTM2 and OsloCTM3 have very high dry  $\text{NO}_3^-$  depositions (Figure 6) compared  
533 with CASTNET observations. The overall high dry and wet  $\text{NO}_3^-$  depositions along with  
534 high atmospheric concentrations (Figure 4a) indicate that the chemical formation of  
535  $\text{NO}_3^-$  in the two models must be also high. This performance might be also true on global  
536 scale since the inferred chemical productions of  $\text{NO}_3^-$  in the two models are the highest  
537 (Table 4a). CHASER has the lowest  $\text{tNH}_4^+$  wet deposition. This may result in a very high  
538  $\text{NH}_4^+$  dry deposition (Figure 6) and concentration (Figures 4a-c, 5) compared with  
539 observations and other models. Overall, wet deposition seems to be the dominant process  
540 in determining the diversity in  $\text{NH}_3$  and  $\text{NH}_4^+$  lifetime (Table 4b).

541

542 Note that we use the traditional approach of comparing models' grid box mean values  
543 with observations, which does not take into account the impact of the models' horizontal  
544 resolutions in their representation of observations (Schutgens et al., 2016). Since majority  
545 models (except EMEP) have horizontal resolutions around 2-3 degrees, the models grid  
546 box means tend to smooth out extreme (i.e. very low or high) observations.

547 Consequently, the slopes of the fitting lines are generally less than 1 on the scattering  
548 plots with model as y-axis and observation as x-axis (e.g. Figures 4a-d, 6, 7a-b).

549

### 550 **5. Discussion of major uncertainties in nitrate formation**

551 Large uncertainties of nitrate studies result from the complexity of the simulations which

552 must consider a comprehensive NO<sub>x</sub>-NMHC-O<sub>3</sub>-NH<sub>3</sub> chemistry and a thermodynamic  
 553 equilibrium model (TEQM) to partition semi-volatile ammonium nitrate between the gas  
 554 and aerosol phases. Nitrate aerosol concentrations depend on temperature, relative  
 555 humidity (RH), and concentrations of HNO<sub>3</sub>, NH<sub>3</sub>, NH<sub>4</sub><sup>+</sup>, SO<sub>4</sub><sup>2-</sup>, Cl<sup>-</sup>, Na<sup>+</sup>, Ca<sup>2+</sup>, K<sup>+</sup>,  
 556 Mg<sup>2+</sup>, organic acids, among others. A further complicating factor is that the equilibrium  
 557 for the coarse mode is somewhat questionable (Feng and Penner, 2007). In addition, wet  
 558 removal of NH<sub>3</sub> is very sensitive to the pH in cloud water. We will discuss some of these  
 559 uncertainties below.

560

### 561 **5.1 pH-dependent NH<sub>3</sub> wet deposition**

562 Gas tracer NH<sub>3</sub>, a precursor of ammonium aerosol, experiences atmospheric wet  
 563 deposition and its deposition rate is typically calculated using Henry's Law. Henry's law  
 564 constant (H) of gases in water is usually given at 298 K (indicated by Θ in superscript)  
 565 and can be adjusted by temperature (T).

$$H(T) = H^{\Theta} * \exp\left(-\frac{\Delta H_{sol}}{R} \left(\frac{1}{T} - \frac{1}{T^{\Theta}}\right)\right) \quad (1)$$

566 Here ΔH<sub>sol</sub> is the enthalpy of dissolution and R is the gas constant.

567

568 For some acidic/basic gases, including NH<sub>3</sub>, Henry's law constant is also a function of  
 569 pH in cloud water (a.k.a effective Henry's law constant H<sup>Θ\*</sup>). As explained in the  
 570 Appendix, the H<sup>Θ\*</sup> is inferred from H<sup>Θ</sup> with a correction of pH (pH = -log<sub>10</sub>[H<sup>+</sup>]) as

$$H^{\Theta*} = H^{\Theta} \frac{K_{al}[H^+]}{K_w} \quad (5)$$

571 Here, K<sub>al</sub> ≈ 1.8x10<sup>-5</sup> and K<sub>w</sub> = 1.0x10<sup>-14</sup> at 298 K in pure water (see Appendix). However,  
 572 not every model accounts for pH adjustment (i.e. the reaction of equation 2 in Appendix)  
 573 for NH<sub>3</sub> dissolution. More accurately, the EMAC model implicitly calculates the  
 574 effective Henry's law constant by solving a set of partial differential equations, which  
 575 includes not only the gas-liquid phase equilibria, but also the reactions in the liquid phase  
 576 (i.e. dissociation or acid-base equilibria, Redox reactions and photolysis reactions in the  
 577 liquid phase, see Tost et al.(2006)). Therefore, the gas-liquid phase equilibrium is  
 578 explicitly calculated based on the chemical mechanism used in the liquid phase. As listed  
 579 in Table 5, the rest of the models are generally divided into two groups based on their  
 580 effective Henry's law constant: (1) INCA, GISS-OMA and GISS-MATRIX has H<sup>Θ\*</sup> ≤  
 581 100 (L-theta without pH correction) and (2) CHASER, GMI, OsloCTM2 and Oslo-  
 582 CTM3 has H<sup>Θ\*</sup> > 10<sup>+5</sup> (H-theta with pH correction). The NH<sub>3</sub>'s H<sup>Θ\*</sup> adopted by the  
 583 models varies dramatically, up to an order of 6 in magnitude among all the models and a  
 584 factor of 10 just for the models in H-theta group (Table 5). The latter corresponds to a  
 585 range of pH from 4.5 (Oslo-CTM2) to 5.5 (CHASER).

586

587 To examine how sensitive of NH<sub>3</sub>, NH<sub>4</sub><sup>+</sup> and NO<sub>3</sub><sup>-</sup> simulations in response to the  
 588 magnitude of NH<sub>3</sub>'s H<sup>Θ\*</sup>, we performed a sensitivity experiment, named TWET, in the  
 589 GMI model in which there was no pH adjustment for NH<sub>3</sub> Henry's law constant (i.e.  
 590 H<sup>Θ\*</sup>=61 instead of 1.05e+6, see table 6). The resultant annual budgets of dry/wet  
 591 deposition, chemistry production and loss, and atmospheric loading of NH<sub>3</sub>,  
 592 NH<sub>4</sub><sup>+</sup> and NO<sub>3</sub><sup>-</sup> are summarized in Table 7, the tracers' vertical zonal mean distributions  
 593 are shown in Figure 8, and the comparisons with the ARCTAS measurements for

594  $\text{NH}_4^+$  and  $\text{NO}_3^-$  are shown in Figure 9. For convenient comparison, the GMI baseline  
595 results are given in the table and figures as well. There is a dramatic decrease (from 17.5  
596 to 1.1 Tg) in  $\text{NH}_3$  wet deposition when using pure water  $\text{NH}_3$  Henry's law constant.  
597 Consequently,  $\text{NH}_3$  will remain in the atmosphere (i.e.  $\sim 8$  times more atmospheric  $\text{NH}_3$ )  
598 to produce  $\sim 1.6$  times more  $\text{NH}_4^+$  chemically. This, in turn, greatly increases atmospheric  
599  $\text{NO}_3^-$  to 0.97 Tg from 0.26 Tg reported in baseline simulation. A large portion of the  
600 increased  $\text{NH}_3$ ,  $\text{NH}_4^+$  and  $\text{NO}_3^-$  resides in the upper troposphere and close to the  
601 tropopause region, while the changes of the tracers in the lower troposphere are relatively  
602 small, as shown in Figure 8. These accumulations at high altitudes are far above (i.e.  $\sim 50$   
603 times for  $\text{NH}_4^+$  and  $\text{NO}_3^-$ ) the ARCTAS observed tracer amounts as shown in Figure 9.  
604 The TWET experiment might be an explanation of  $\text{NH}_4^+$  and  $\text{NO}_3^-$  accumulations near the  
605 tropopause region (Figure 3a-b) in the INCA model whose  $\text{NH}_3$  Henry's law constant  $H^\ominus$   
606 is 74 without pH correction (i.e. a L-theta model, table 5). However, it is puzzling that the  
607  $\text{NH}_3$  simulations by GISS-MATRIX and GISS-OMA, those are the models with L-theta,  
608 are closer to the simulations of the models with H-theta, i.e. no  $\text{NH}_4^+$  and  $\text{NO}_3^-$   
609 accumulation near the tropopause and comparable removal of  $\text{NH}_4^+$  (Figure 3a-b and  
610 Table 4b).

611

## 612 **5.2 Contribution of dust and sea salt on nitrate formation**

613 In the presence of acidic accumulation-mode sulfuric acid containing aerosols,  $\text{HNO}_3$ ,  
614  $\text{NO}_3$  radicals, and  $\text{N}_2\text{O}_5$  will deposit on larger alkaline mineral or salt particles (Dentener  
615 et al., 1996; Gard et al., 1998; Hauglustaine 2014; Karydis et al., 2016; Murphy and  
616 Thomson 1997; Paulot et al., 2016). Considerable evidence shows that the majority of  
617 atmospheric nitrate is formed via reactions associated with dust and sea salt (Allen et al.  
618 2015; Itahashi et al., 2016; Karydis et al., 2016). Coarse mode nitrate overwhelmingly  
619 dominates over remote oceanic regions (Itahashi et al., 2016). Over wide land regions,  
620 nitrate also quite often exists in the form of supermicron  $\text{NO}_3^-$  balanced by the presence  
621 of mineral cations arising from transport of crustal dust and sea spray aerosol (Allen et  
622 al., 2015; Lefer and Talbot, 2001).

623

624 Investigation of nitrate interactions with mineral dust and sea salt depends on the  
625 simulation approach adopted in a model. The traditional equilibrium approach to partition  
626 semi-volatile  $\text{HNO}_3$  between the gas and aerosol phases is no longer possible since the  
627 time to reach equilibrium on coarse mode particles (several hours to days) is typically  
628 much longer than the chemical time step used in a global model (less than 1 hour) (John  
629 et al., 1989; Myhre et al., 2006). Meng and Seinfeld (1996) found that on longer time  
630 scales, when  $\text{NH}_3/\text{HNO}_3$  started to condense on larger aerosols, their gas phase  
631 concentrations decreased so that some of the condensed matter can be driven back to the  
632 gas phase from the small semi-volatile aerosols. A fix to a non-equilibrium state would  
633 be to implement a kinetic formulation for the particles that have a long equilibrium time  
634 scale (Feng and Penner, 2007; Karydis et al., 2010). However, implementing explicit  
635 kinetics in a global model would be computationally expensive and, hence, is not feasible  
636 for long-term climate simulations. Several approximations have been developed to allow  
637 computational efficiency although they might compromise model accuracy

638

639 Four such approximations are adopted by the nine models participating in this study: 1)

640 using equilibrium calculations for fine mode particles only while neglecting nitrate  
641 formation on coarse mode particles (CHASER and GISS-MATRIX); 2) combining  
642 equilibrium calculation for a solution of  $\text{SO}_4^{2-}$ - $\text{NO}_3^-$ - $\text{NH}_4^+$ - $\text{H}_2\text{O}$  and heterogeneous  
643 reaction calculation for nitrogen uptake on dust and sea-salt using a first-order loss rate  
644 (EMEP, GMI, GISS-OMA and INCA); 3) running equilibrium model including  $\text{NH}_3$ ,  
645 dust and sea salt repeatedly for aerosol sizes from fine mode to coarse mode (Oslo-CTM2  
646 and Oslo-CTM3); and 4) using only the fraction of the gas that can kinetically condense  
647 within the time step of the model in the equilibrium calculations for each aerosol size  
648 mode (EMAC).

649  
650 Nitrate is formed primarily on dust and sea salt by GMI (88%) and INCA (82%) (see  
651 Table 4a). INCA further separates the formation as 45% on dust and 37% on sea-salt. The  
652 above-mentioned approach 1 is problematic due to absence of coarse mode nitrate, an  
653 important portion of nitrate, which results in relatively low nitrate burdens for CHASER  
654 and GISS-MATRIX. Unfortunately, the other models are missing a detailed nitrate  
655 chemistry budget report. A potential impact of dust and sea-salt on nitrate formation,  
656 nevertheless, can be inferred from the approach adopted by a model. For example,  
657 OsloCTM2 and OsloCTM3 adopt approach 3. Although the model allows fine mode  
658 particles to reach equilibrium first, the subsequent equilibrium calculation for coarse  
659 mode particles may still produce coarse mode nitrate too quickly, see discussion of the  
660 ratio of coarse model nitrate in the next subsection. To avoid such overestimations on the  
661 production of coarse mode nitrate, EMAC allows only a fraction of  $\text{HNO}_3$  to partition in  
662 the aerosol phase by assuming diffusion limited condensation (Pringle et al., 2010).

663  
664 To further understand the role of homogeneous and heterogeneous chemical reaction  
665 processes in nitrate formation, we conducted two more sensitivity experiments,  
666 TnoCNH3 and TnoCHET, with the GMI model (Table 6). Experiment TnoCNH3 turned  
667 off chemical conversion of  $\text{NH}_3$  to  $\text{NH}_4^+$  in the GMI thermodynamic equilibrium model,  
668 while experiment TnoCHET excluded the nitrate formation via heterogeneous reaction of  
669 gas  $\text{HNO}_3$  on the particles of dust and sea salt. The budget report, vertical zonal mean  
670 distribution and model-observation comparison of  $\text{NH}_3$ ,  $\text{NH}_4^+$  and  $\text{NO}_3^-$  are given in Table  
671 7 and Figures 8-9, respectively. It is not surprising that experiment TnoCNH3 gives a  
672 higher atmospheric  $\text{NH}_3$  burden (0.32 Tg) compared with baseline (0.11 Tg) with little  
673  $\text{NH}_4^+$  left (from its initial field). The interesting thing is that the formed  $\text{NO}_3^-$  has only  
674 slightly decreased compared with baseline (from 0.26 to 0.20 Tg), confirming the  
675 importance of  $\text{NO}_3^-$  formation via dust and sea salt. For experiment TnoCHET, the  
676 simulations of  $\text{NH}_3$  and  $\text{NH}_4^+$  stay the same but the formed  $\text{NO}_3^-$  is decreased dramatically  
677 (from 0.26 to 0.10), indicating that  $\text{NO}_3^-$  formation via  $\text{NH}_3$  chemistry alone in the GMI  
678 model is relatively small. The chemical production of  $\text{NO}_3^-$  is about 6 times larger in  
679 TnoCNH3 (via dust and sea salt) than in TnoCHET (via  $\text{NH}_3$ ). However, the  $\text{NO}_3^-$   
680 produced via  $\text{NH}_3$  chemistry (TnoCHET) is non-negligible over remote regions impacted  
681 by long-range transport, as shown in the analysis of April Alaska observations in Figure  
682 9.

### 683 684 **5.3 Nitrate size distribution**

685 Unlike sulfate aerosol, a noticeable fraction of nitrate aerosol is in coarse mode. Coarse

686 mode aerosol nitrate is formed due to presence of dust and/or sea salt. In other words, the  
687 formation of nitrate on coarse mode dust and sea salt particles is the major factor  
688 controlling size distribution. Other factors, such as  $\text{NH}_3/\text{NH}_4^+/\text{NO}_3^-$  chemistry and  
689 atmospheric transport and removal processes, also affect nitrate size distribution. Having  
690 an accurate aerosol size distribution is critical in climate forcing estimations, since large  
691 size particles have a relatively small optical cross section at a given aerosol mass loading  
692 and the nitrate material coating on dust particles has almost no direct impact on the dust  
693 optics, although the greatly impact dust lifetime (Bauer et al., 2007). Given that the  
694 deposition velocity of a coarse particle is greater than that of a fine particle, an accurate  
695 size distribution is also necessary to estimate deposition of particulate nitrates (Yeatman  
696 et al., 2001; Sadanaga et al., 2008). This estimation is particularly important over oceans  
697 where coarse mode nitrate dominates (Itahashi et al., 2016) and nitrogen supply is often  
698 in deficit (Hansell and Follows, 2008).

699  
700 As we have discussed in section 5.2, nitrate size distribution varies with the approaches  
701 adopted for nitrate formation on coarse mode aerosols (i.e. dust and sea salt). Figure 10  
702 gives the burdens of nitrate in fine mode and coarse mode portions and the ratio between  
703 coarse mode and total ( $f_c$ ) for the eight discussed models. The ratio is ranging from 0  
704 (CHASER and GISS-OMA), ~50% (EMAC, GMI and INCA), ~80% (EMEP and  
705 OsloCTM2), and 97% (OsloCTM3). The two OsloCTMs give the highest  $f_c$  partially  
706 because they run TEQM model for coarse model particles.

707  
708 A wide range of  $f_c$ , from 0 to > 90%, has been reported previously by model  
709 simulations (Adams et al., 2001; Bauer et al., 2007; Jacobson 2001), while the range is  
710 narrowed down to 40-60% for the model studies using the approach that solves dynamic  
711 mass transfer equation for coarse mode particles (Feng and Penner, 2007; Xu and Penner,  
712 2012).

713  
714 It is worth pointing out that aerosol microphysics modify aerosol size as well. For  
715 example, a process like coagulation would also allow  $\text{NO}_3^-$  to mix with other particles and  
716 enter coarse mode aerosol. New particle formation/nucleation would add  $\text{NH}_3/\text{NH}_4^+/\text{NO}_3^-$   
717 into the ultra fine mode. Except EMAC and GISS-MATRIX, majority models involved in  
718 this study are bulk aerosol models that do not account for aerosol microphysics.

719  
720 It is challenging to verify the nitrate size distribution globally due to the limited  
721 measurements on time and space. Measurements over regional and station sites indicated  
722 that the ratio of  $f_c$  could be very high and vary seasonally over oceanic sites. For  
723 example, annual mean  $f_c$  during 2002-2004 from the Fukue supersite observatory is  
724 about 72% with a seasonal variation of 60–80% in winter and of around 80% in summer  
725 (Itahashi et al., 2016).

726  
727 However, the ratio could be varied dramatically over land or the areas affected by land  
728 pollution. For example, observations of fine and coarse particulate nitrate at several rural  
729 locations in the United States indicated that nitrate was predominantly in submicron  
730 ammonium nitrate particles during the Bondville and San Gorgonio (April) campaigns, in  
731 coarse mode nitrate particles at Grand Canyon (May) and Great Smoky Mountains



732 (July/August), and both fine and coarse mode nitrate during the studies at Brigantine and  
733 San Gorgonio (July) (Lee et al., 2008). Allen et al. (2015) examined aerosol composition  
734 data collected during the summer 2013 SOAS and concluded that inorganic nitrate in the  
735 southeastern United States likely exists in the form of supermicron  $\text{NO}_3^-$ , balanced by the  
736 presence of mineral cations arising from the transport of crustal dust and sea spray  
737 aerosol. The measurements over Harvard Forest, a rural site in central Massachusetts,  
738 supported that the majority of nitrate mass was associated with water-soluble  
739 supermicron soil-derived  $\text{Ca}^{2+}$  in an acidic environment (Lefer and Talbot, 2001).  
740 Measurements taken in Paris during the ESQUIF campaign found that the coarse  
741 nitrate fraction represents up to 60% of total particulate nitrate mass at night and 80% at  
742 day (Hodzic et al., 2006a, 2006b). Measurements of coarse-mode aerosol nitrate and  
743 ammonium at two polluted coastal sites, Weybourne, England and Mace Head, Ireland,  
744 during polluted flow when the air had passed over strong source regions of the UK and  
745 northern Europe, showed 40–60% of the nitrate was found in particles with diameter  
746  $>1 \mu\text{m}$ , but under clean marine conditions almost 100% conversion was seen (Yeatman et  
747 al., 2001).

748

## 749 **6. Conclusions**

750

751 We present the AeroCom phase III nitrate study by assessing aerosol simulations of  
752 nitrate and ammonium and their precursors with nine global models. Five of the models  
753 couple the chemical calculation online with meteorological simulation, and four use  
754 archived meteorological fields driving chemistry. To focus on chemical-physical  
755 processes behind the diversity of nitrate simulation, all participating models are  
756 encouraged to use HTAP2 emission inventory for aerosol and gas emissions from  
757 anthropogenic, aircraft, and ship sources. The simulated aerosols of nitrate and  
758 ammonium and their precursors are compared among the models and evaluated against  
759 various measurements including surface concentrations and dry/wet depositions from  
760 surface measurements, and vertical distributions from aircraft measurements.

761

762 All models capture the main features of the distribution of nitrate and ammonium: large  
763 surface and column amounts over China, South Asia, Europe, and U.S. These regions are  
764 typically densely populated with large  $\text{NH}_3$  and  $\text{NO}_x$  emissions. Many models also show  
765 enhanced nitrate and ammonium over the Middle East and continents over the Southern  
766 Hemisphere. The former undergoes huge dust pollution and the latter experiences fires  
767 that emit both  $\text{NH}_3$  and  $\text{NO}_x$ .

768

769 The diversity of nitrate and ammonium simulations among the models is large: the ratio  
770 of the maximum to minimum quantities among the nine models is 13.4 and 4.4 for model  
771 simulated global mass burdens of nitrate and ammonium, respectively, and 3.9 and 5.2  
772 for the corresponding lifetimes. These values are also larger than those of sulfate: 4.0 for  
773 global burden and 3.0 for lifetime. The agreement between models and observations is  
774 better for aerosol components than for gas tracers. All models underestimate  $\text{NH}_3$  surface  
775 mass concentrations but most models overestimate surface  $\text{HNO}_3$  concentrations over  
776 North America and East Asia. Performance of  $\text{NH}_3$  is the worst: this could partially be  
777 associated to its relatively lower measurement accuracy, i.e. a loss of ammonia possibly

778 on the filters designed to collect  $\text{NH}_3$  (Williams et al., 1992). Among aerosol simulations,  
779 model performance based on evaluation of surface mixing ratio and dry/wet depositions  
780 is very similar for  $\text{NH}_4^+$  and  $\text{SO}_4^{2-}$ , while slightly worse for  $\text{NO}_3^-$ . Models severely  
781 underestimate the aerosol concentrations with only a few exceptions when compared with  
782 aircraft measurements and this problem is worse over regions impacted by long-range  
783 transport than those closer to sources.

784

785 There are many intrinsic reasons for a larger diversity in nitrate simulations among  
786 models. Nitrate is involved in much more complicated chemistry: the chemical  
787 mechanism needs to handle a multiphase multicomponent solution system. The system  
788 sometimes cannot even be solved using the thermodynamic equilibrium approach when  
789 coarse mode dust and sea salt particles present. A reasonable nitrate simulation also  
790 depends on good simulations of various precursors, such as  $\text{NH}_3$ ,  $\text{HNO}_3$ , dust and sea  
791 salt, although models account for impact of dust and sea salt very differently. Even an  
792 accurate simulation of  $\text{SO}_4^{2-}$  is a prerequisite because  $\text{SO}_4^{2-}$  surpasses  $\text{NO}_3^-$  at reacting  
793 with  $\text{NH}_4^+$ .

794

795 The models' intercomparison and model-observation comparison revealed at least two  
796 critical issues in nitrate simulation that demand further exploration:  $\text{NH}_3$  wet deposition  
797 and relative contribution to  $\text{NO}_3^-$  formation via  $\text{NH}_3$  and dust/sea salt. The nine  
798 participating models adopt very different effective Henry's law constants for  $\text{NH}_3$ , with  
799 one group having a value equal or less than 100 (in pure water) and the other larger than  
800  $1.e+05$  (with pH correction). Sensitivity studies using the GMI model indicated that  
801 without pH correction,  $\text{NH}_3$  wet deposition decreases massively (from 17.5 to 1.1 Tg),  
802 which prolongs atmospheric  $\text{NH}_3$  lifetime (from 0.67 to 5.2 days) and enhances its  
803 atmospheric burden (from 0.11 to 0.85 Tg), and thus the atmospheric burden of  $\text{NH}_4^+$   
804 (from 0.17 to 0.48 Tg) and  $\text{NO}_3^-$  (from 0.26 to 0.97 Tg) as well. These enhanced tracers  
805 tend to accumulate in the upper troposphere and close to the tropopause, and are too high  
806 when compared with aircraft measurements. Since liquid-phase reaction 2 in Appendix  
807 can reach equilibrium quickly within a chemical time step, we recommend including it in  
808 accounting for  $\text{NH}_3$  solution. Theoretically, a more accurate approach is to combine wet  
809 removal with liquid-phase chemistry calculation. In other words, instead of using an  
810 implicit calculation of effective Henry's law constant, the gas-liquid phase equilibrium is  
811 explicitly calculated based on the chemical mechanism used in the liquid phase. The  
812 solution of  $\text{NH}_3$  is calculated by solving a set of partial differential equations, which  
813 includes not only the gas-liquid phase equilibrium, but also all the important reactions in  
814 the liquid phase, as adopted in EMAC model.

815

816 All the models use thermodynamic equilibrium to solve the chemical process of  
817  $\text{NH}_3/\text{NH}_4^+$  to  $\text{NO}_3^-$  formation in fine mode aerosols. However, the models adopt very  
818 different ways in accounting for the contribution of these reactions on the surface of dust  
819 and sea salt particles: some account for both dust and sea salt, some account for only dust  
820 or only sea salt, and two models even do not account for dust and sea salt. The  
821 methodologies that take dust and sea salt into account are also very different, i.e. together  
822 with  $\text{NH}_4^+$  using thermodynamic equilibrium model or simply adopting a first order loss  
823 rate on dust and sea salt surfaces. The chemical budget reported by GMI and INCA

824 indicates that the majority (>80%) of global  $\text{NO}_3^-$  formation is via reaction on dust and  
825 sea salt. Two sensitivity experiments using the GMI model by tagging the  $\text{NO}_3^-$  formation  
826 from either  $\text{NH}_3/\text{NH}_4^+$  chemistry or heterogeneous reactions on dust and sea salt confirm  
827 the critical importance of the latter process, and indicate that the former process is  
828 relatively important in remote regions. The importance of  $\text{NO}_3^-$  formation on dust and sea  
829 salt lies also in its determination on nitrate particle size distribution, so that has an  
830 implication in air quality and climate studies as well.

831

832 Our work presents a first effort to assess nitrate simulation from chemical (e.g. chemistry  
833 among  $\text{NH}_3$ ,  $\text{NH}_4^+$ ,  $\text{NO}_3^-$ ,  $\text{SO}_4^{2-}$ , dust and sea salt) and physical processes (e.g emission,  
834 dry deposition, and wet deposition). A companion study is proposed by AeroCom III  
835 nitrate activity to investigate how sensitive nitrate formation is in response to possible  
836 future changes in emission and meteorological fields. These perturbation fields include  
837 increasing  $\text{NH}_3$  emission, decreasing  $\text{NO}_x$ ,  $\text{SO}_x$ , and dust emissions, and increasing  
838 atmospheric temperature and relative humidity. It would be particularly interesting to  
839 examine how aerosol pH changes and its influence on atmospheric acid/base gas-particle  
840 system. Future aerosol pH does not necessarily increase with  $\text{SO}_2$  emission reduction.  
841 Indeed, studies over US southeast indicated that its aerosol has become more acidic over  
842 the past decade although  $\text{SO}_2$  emission decreased and  $\text{NH}_3$  emission stayed constant  
843 [Silvern et al., 2017; Weber et al., 2016]. This environment of high aerosol acidity  
844 hinders the formation of nitrate aerosol, which only occurs when pH is over ~2 to 3  
845 [Weber et al., 2016]. In addition, understanding why and how the system is insensitive to  
846 changing  $\text{SO}_2$  level due to buffering of the partitioning of semivolatile  $\text{NH}_3$  helps us to  
847 gain insight into how errors in sulfate (and ammonium) may propagate to errors in  
848 aerosol nitrate. In particular, the correlation between model predictions and observations  
849 for  $\text{SO}_4^{2-}$  and  $\text{NH}_4^+$  is quite poor for some models (Figure 4). It would also be interesting  
850 to include organic gas/aerosol in the system since they are not only important  
851 atmospheric components, but also reduce the uptake of  $\text{NH}_3$ . Competition for uptake  
852 between  $\text{NH}_3$  and organic gases considerably slows down the approach to  
853 thermodynamic equilibrium [Silvern et al., 2017]. Based on the findings of this work,  
854 modelers should pay particular attention to incorporating dust and sea salt and treating  
855  $\text{NH}_3$  wet deposition to improve nitrate simulation. Further evaluation using satellite  
856 measurements, such as  $\text{NH}_3$  products from IASI and TES, is desired and will be  
857 conducted. Such evaluation requires global 3-dimensional high frequency model data.  
858 Potential future study also includes estimation of nitrate forcing for climate change.

859

## 860 **Appendix**

861 For some acidic/basic gases, including  $\text{NH}_3$ , Henry's law constant is also a function of  
862 pH in water (a.k.a effective Henry's law constant). This is because not only does the  
863 aqueous chemistry reaction  $\text{NH}_3 + \text{H}_2\text{O}$  (equation 1) reach equilibrium within a chemical  
864 time step but its product  $\text{NH}_3 \cdot \text{H}_2\text{O}$  (equation 2) does as well.



865 Here,  $\text{NH}_4^+$  is the ammonium ion and  $\text{OH}^-$  is the hydroxide ion. The total dissolved  
866 ammonia  $[\text{NH}_3^T]$  is given by

$$[\text{NH}_3^T] = [\text{NH}_3 \cdot \text{H}_2\text{O}] + [\text{NH}_4^+]$$

$$\begin{aligned}
&= p_{\text{NH}_3} H^\ominus \left( 1 + \frac{K_{\text{al}}[\text{H}^+]}{K_w} \right) \\
&\approx p_{\text{NH}_3} \left( H^\ominus \frac{K_{\text{al}}[\text{H}^+]}{K_w} \right) \quad (3)
\end{aligned}$$

867 Here,  $p_{\text{NH}_3}$  is the partial pressure of  $\text{NH}_3$ ,  $K_{\text{al}} = [\text{NH}_4^+][\text{OH}^-] / [\text{NH}_3 \cdot \text{H}_2\text{O}] \approx 1.8 \times 10^{-5}$ , and  
868  $K_w = 1.0 \times 10^{-14}$  at 298 K in pure water. So the effective Henry's law constant  $H^{\ominus*}$  is  
869 inferred from  $H^\ominus$  with a correction of pH ( $\text{pH} = -\log_{10}[\text{H}^+]$ ) as

$$H^{\ominus*} = H^\ominus \frac{K_{\text{al}}[\text{H}^+]}{K_w} \quad (4)$$

870

## 871 References:

- 872 Allen, H. M., D. C. Draper, B. R. Ayres, A. Ault, A. Bondy, S. Takahama, R. L. Modini, K. Baumann, E.  
873 Edgerton, C. Knute, A. Laskin, B. Wang, and J. L. Fry, Influence of crustal dust and sea spray  
874 supermicron particle concentrations and acidity on inorganic  $\text{NO}_3$  aerosol during the 2013 Southern  
875 Oxidant and Aerosol Study, *Atmos. Chem. Phys.*, 15, 10669–10685, 2015, [www.atmos-chem-](http://www.atmos-chem-phys.net/15/10669/2015/)  
876 [phys.net/15/10669/2015/](http://www.atmos-chem-phys.net/15/10669/2015/), doi:10.5194/acp-15-10669-2015.
- 877 Bauer, S. E., Balkanski, Y., Schulz, M., Hauglustaine, D. A., and Dentener, F.: Global modeling of  
878 heterogeneous chemistry on mineral aerosol surfaces: Influence on tropospheric ozone chemistry and  
879 comparison to observations, *J. Geophys. Res.-Atmos.*, 109, D02304, doi:10.1029/2003jd003868, 2004.
- 880 Bauer, S.E., and D. Koch, 2005: Impact of heterogeneous sulfate formation at mineral dust surfaces on  
881 aerosol loads and radiative forcing in the Goddard Institute for Space Studies general circulation  
882 model. *J. Geophys. Res.*, 110, D17202, doi:10.1029/2005JD005870.
- 883 Bauer, S. E., Koch, D., Unger, N., Metzger, S. M., Shindell, D. T., and Streets, D. G.: Nitrate aerosols  
884 today and in 2030: a global simulation including aerosols and tropospheric ozone, *Atmos. Chem.*  
885 *Phys.*, 7, 5043–5059, doi:10.5194/acp-7-5043-2007, 2007.
- 886 Bauer, S.E., D. Wright, D. Koch, E.R. Lewis, R. McGraw, L.-S. Chang, S.E. Schwartz, and R. Ruedy,  
887 2008: MATRIX (Multiconfiguration Aerosol TRacker of mIXing state): An aerosol microphysical  
888 module for global atmospheric models. *Atmos. Chem. Phys.*, 8, 6603-6035, doi:10.5194/acp-8-6003-  
889 2008.
- 890 Bauer, S. E., K. Tsigaridis, and R. Miller, Significant atmospheric aerosol pollution caused by world food  
891 cultivation, *Geophys. Res. Lett.*, 43, no. 10, 5394-5400, doi:10.1002/2016GL068354, 2016.
- 892 Bessagnet, B. and Rouil, L.: Feedback on and analysis of the PM pollution episode in March 2014,  
893 presentation at 19-th EIONET Workshop on Air Quality Assessment and Management Berne,  
894 Switzerland, 30 September and 1 October 2014, 2014.
- 895 Bey, I, D.J. Jacob, R.M. Yantosca, J.A. Logan, B.D. Field, A.M. Fiore, Q. Li, H.Y. Liu, L.J. Mickley, M.G.  
896 Schultz, 2001: Global modeling of tropospheric chemistry with assimilated meteorology: Model  
897 description and evaluation. *J. Geophys. Res.*, 106, 23073-23078 (2001JD000807).
- 898 Bellouin, N., Rae, J., Jones, A., Johnson, C., Haywood, J., and Boucher, O.: Aerosol forcing in the Climate  
899 Model Intercomparison Project (CMIP5) simulations by HadGEM2-ES and the role of ammonium  
900 nitrate, *J. Geophys. Res.-Atmos.*, 116, D20206, doi:10.1029/2011jd016074, 2011.
- 901 Berntsen, T. K. and Isaksen, I. S. A.: A global three-dimensional chemical transport model for the  
902 troposphere. I. Model description and CO and ozone results, *J. Geophys. Res.-Atmos.*, 102(D17), 21  
903 239–21 280, 1997.
- 904 Bian, H., and C. S. Zender (2003), Mineral dust and global tropospheric chemistry: The relative roles of  
905 photolysis and heterogeneous uptake. *J. Geophys. Res.*, 108, 4672.
- 906 Bian, H., Chin, M., Rodriguez, J. M., Yu, H., Penner, J. E., and Strahan, S., 2009: Sensitivity of aerosol  
907 optical thickness and aerosol direct radiative effect to relative humidity, *Atmos. Chem. Phys.*, 9, 2375-  
908 2386, doi:10.5194/acp-9-2375-2009.
- 909 Bian, H., Colarco, P. R., Chin, M., Chen, G., Rodriguez, J. M., Liang, Q., Blake, D., Chu, D. A.,  
910 da Silva, A., Darmenov, A. S., Diskin, G., Fuelberg, H. E., Huey, G., Kondo, Y., Nielsen, J. E.,  
911 Pan, X., and Wisthaler, A.: Source attributions of pollution to the Western Arctic during the NASA  
912 ARCTAS field campaign, *Atmos. Chem. Phys.*, 13, 4707-4721, doi:10.5194/acp-13-4707-2013, 2013.

913 Bouwman, A.F., Lee, D.S., Asman, W.A.H., Dentener, F.J., Van Der Hoek, K.W. and J.G.J. Olivier (1997).  
914 A Global High-Resolution Emission Inventory for Ammonia, *Global Biogeochemical Cycles*, 11:4,  
915 561-587. <http://www.rivm.nl/>.

916 Chin, M., P. Ginoux, S. Kinne, B. N. Holben, B. N. Duncan, R. V. Martin, J. A. Logan, A. Higurashi, and  
917 T. Nakajima, 2002: Tropospheric aerosol optical thickness from the GOCART model and comparisons  
918 with satellite and sun photometer measurements, *J. Atmos. Sci.* 59, 461-483.

919 Cubison, M. J., Ortega, A. M., Hayes, P. L., Farmer, D. K., Day, D., Lechner, M. J., Brune, W. H., Apel,  
920 E., Diskin, G. S., Fisher, J. A., Fuelberg, H. E., Hecobian, A., Knapp, D. J., Mikoviny, T., Riemer, D.,  
921 Sachse, G. W., Sessions, W., Weber, R. J., Weinheimer, A. J., Wisthaler, A., and Jimenez, J. L.:  
922 Effects of aging on organic aerosol from open biomass burning smoke in aircraft and laboratory  
923 studies, *Atmos. Chem. Phys.*, 11, 12049–12064, doi:10.5194/acp-11-12049-2011, 2011.

924 Davis, J. M., P. M. Bhawe, and K. M. Foley (2008), Parameterization of N<sub>2</sub>O<sub>5</sub> reaction probabilities on the  
925 surface of particles containing ammonium, sulfate and nitrate, *Atmos. Chem. Phys.*, 8, 5295 – 5311.

926 DeCarlo, P. F., Kimmel, J. R., Trimborn, A., Northway, M. J., Jayne, J. T., Aiken, A. C., Gonin, M.,  
927 Fuhrer, K., Horvath, T., Docherty, K. S., Worsnop, D. R., and Jimenez, J. L.: Field-deployable, high-  
928 resolution, time-of-flight aerosol mass spectrometer, *Anal. Chem.*, 78(24), 8281–8289, 2006.

929 Dentener, F. J., G. R. Carmichael, Y. Zhang, J. Lelieveld, and P. J. Crutzen, Role of mineral aerosol as a  
930 reactive surface in the global troposphere, *J. Geophys. Res.*, 101, 22,869-22889, 1996.

931 Dentener, F. and Crutzen, P.: Reaction of NO on Tropospheric Aerosols: Impact on the Global  
932 Distributions of NO, O, and OH, *J. Geophys. Res.*, 98, 7149–7163, doi:10.1029/92JD02979, 1993.

933 Dentener, F., Kinne, S., Bond, T., Boucher, O., Cofala, J., Generoso, S., Ginoux, P., Gong, S., Hoelzemann,  
934 J. J., Ito, A., Marelli, L., Penner, J. E., Putaud, J.-P., Textor, C., Schulz, M., van der Werf, G. R., and  
935 Wilson, J.: Emissions of primary aerosol and precursor gases in the years 2000 and 1750 prescribed  
936 data-sets for AeroCom, *Atmos. Chem. Phys.*, 6, 4321–4344, doi:10.5194/acp-6-4321-2006, 2006.

937 Evans, M. J. and Jacob, D. J.: Impact of new laboratory studies of N<sub>2</sub>O<sub>5</sub> hydrolysis on global model  
938 budgets of tropospheric nitrogen oxides, ozone and OH, *Geophys. Res. Lett.*, 32, L09813,  
939 doi:10.1029/2005GL022469, 2005.

940 Ensberg, J. J., Craven, J. S., Metcalf, A. R., Allan, J. D., Angevine, W. M., Bahreini, R., Brioude, J., Cai,  
941 C., Coe, H., de Gouw, J. A., Ellis, R. A., Flynn, J. H., Haman, C. L., Hayes, P. L., Jimenez, J. L.,  
942 Lefer, B. L., Middlebrook, A. M., Murphy, J. G., Neuman, J. A., Nowak, J. B., Roberts, J. M., Stutz, J.,  
943 Taylor, J. W., Veres, P. R., Walker, J. M., and Seinfeld, J. H.: Inorganic and black carbon aerosols in  
944 the Los Angeles Basin during CalNex, *Journal of Geophysical Research-Atmospheres*, 118, 1777-  
945 1803, 2013.

946 Fairlie, T. D., Jacob, D. J., Dibb, J. E., Alexander, B., Avery, M. A., van Donkelaar, A., and Zhang, L.:  
947 Impact of mineral dust on nitrate, sulfate, and ozone in transpacific Asian pollution plumes, *Atmos.*  
948 *Chem. Phys.*, 10, 3999–4012, doi:10.5194/acp-10-3999-2010, 2010.

949 Feng, Y. and Penner, J. E.: Global modeling of nitrate and ammonium: Interaction of aerosols and  
950 tropospheric chemistry, *J. Geophys. Res.-Atmos.*, 112, D01304, doi:10.1029/2005jd006404, 2007.

951 Fenn, M. E., M. A. Poth, D. W. Johnson, Evidence for nitrogen saturation in the San Bernardino Mountains  
952 in southern California, *Forest Ecology and Management*, Volume 82, Issues 1–3, April 1996, Pages  
953 211-230.

954 Fitzgerald, J. W. (1975), Approximation formulas for equilibrium size of an aerosol particle as a function  
955 of its dry size and composition and ambient relative humidity, *J. Appl. Meteorol.*, 14(6), 1044-1049.

956 Fowler, Z. K., M. B. Adams, W. T. Peterjohn, Will more nitrogen enhance carbon storage in young forest  
957 stands in central Appalachia? *Forest Ecology and Management*, Volume 337, Pages 144–152, 1  
958 February 2015.

959 Galloway, J. N., Dentener, F. J., Capone, D. G., Boyer, E. W., Howarth, R. W., Seitzinger, S. P., Asner, G.  
960 P., Cleveland, C. C., Green, P. A., Holland, E. A., Karl, D. M., Michaels, A. F., Porter, J. H.,  
961 Townsend, A. R. and Vorosmarty, C. J.: Nitrogen cycles: Past, present, and future, *Biogeochemistry*,  
962 70, 153–226, 2004.

963 Ginoux, P., M. Chin, I. Tegen, J. Prospero, B. Holben, O. Dubovik, and S.-J. Lin, 2001: Sources and global  
964 distributions of dust aerosols simulated with the GOCART model, *J. Geophys. Res.*, 106, 20,255-  
965 20,273.

966 Grieshop, A. P., Robinson, A. L., Duplissy, J., Smith, J. D., Wilson, K. R., Lanz, V. A., Hueglin, C., Sun,  
967 Y. L., Tian, J., Laaksonen, A., Raatikainen, T., Rautiainen, J., Vaattovaara, P., Ehn, M., Kulmala, M.,  
968 Tomlinson, J. M., Collins, D. R., Cubison, M. J., Dunlea, E. J., Huffman, J. A., Onasch, T. B., Alfarra,

969 M. R., Williams, P. I., Bower, K., Kondo, Y., Schneider, J., Drewnick, F., Borrmann, S., Weimer, S.,  
970 Demerjian, K., Salcedo, D., Cottrell, L., Griffin, R., Takami, A., Miyoshi, T., Hatakeyama, S.,  
971 Shimono, A., Sun, J. Y., Zhang, Y. M., Dzepina, K., Kimmel, J. R., Sueper, D., Jayne, J. T., Herndon,  
972 S. C., Trimborn, A. M., Williams, L. R., Wood, E. C., Middlebrook, A. M., Kolb, C. E., Baltensperger,  
973 U., and Worsnop, D. R.: Evolution of organic aerosols in the atmosphere, *Science*, 326, 1525–1529,  
974 2009.

975 Hansell, D.A., Follows, M.J., 2008. Nitrogen in the Atlantic Ocean. In: Mullholland, M., Bronk, D.,  
976 Capone, D., Carpenter, E. (Eds.), *Nitrogen in the Marine Environment*, second ed. Academic Press, pp.  
977 597–630.

978 Hauglustaine, D. A., Hourdin, F., Walters, S., Jourdain, L., Filiberti, M.-A., Lamarque, J.-F., and Holland,  
979 E. A.: Interactive chemistry in the Laboratoire de Météorologie Dynamique general circulation model:  
980 description and background tropospheric chemistry evaluation, *J. Geophys. Res.*, 109, D04314,  
981 doi:10.1029/2003JD003957, 2004.

982 Hauglustaine, D. A., Balkanski, Y., and Schulz, M.: A global model simulation of present and future  
983 nitrate aerosols and their direct radiative forcing of climate, *Atmos. Chem. Phys.*, 14, 11031–11063,  
984 doi:10.5194/acp-14-11031-2014, 2014.

985 Haywood, J., Bush, M., Abel, S., Claxton, B., Coe, H., Crosier, J., Harrison, M., Macpherson, B., Naylor,  
986 M., and Osborne, S.: Prediction of visibility and aerosol within the operational Met Office Unified  
987 Model II?: Validation of model performance using observational data, *Q. J. Roy. Meteorol. Soc.*, 134,  
988 1817–1832, doi:10.1002/qj.275, 2008.

989 Heald, C. L., Collett Jr., J. L., Lee, T., Benedict, K. B., Schwandner, F. M., Li, Y., Clarisse, L., Hurtmans,  
990 D. R., Van Damme, M., Clerbaux, C., Coheur, P.-F., Philip, S., Martin, R. V., and Pye, H. O. T.:  
991 Atmospheric ammonia and particulate inorganic nitrogen over the United States, *Atmos. Chem. Phys.*,  
992 12, 10295–10312, doi:10.5194/acp-12-10295-2012, 2012.

993 Hess, M., P. Koepke and I. Schult, Optical properties of aerosols and clouds: The software package OPAC.  
994 *Bull. Amer. Meteorol. Soc.*, 79(5): 831-844, 1998.

995 Hodzic, A., R. Vautard, P. Chazette, L. Menut, and B. Bessagnet, Aerosol chemical and optical properties  
996 over the Paris area within ESQUIF project, *Atmos. Chem. Phys.*, 6, 3257 – 3280, 2006a.

997 Hodzic, A., Bessagnet, B., and Vautard, R.: A model evaluation of coarse-mode nitrate heterogeneous  
998 formation on dust particles, *Atmos. Environ.*, 40 4158–4171, 2006b.

999 Huffman, J. A., J. T. Jayne, F. Drewnick, A. C. Aiken, T. Onasch, D. R. Worsnop, and J. L. Jimenez,  
1000 Design, Modeling, Optimization, and Experimental Tests of a Particle Beam Width Probe for the  
1001 Aerodyne Aerosol Mass Spectrometer, *Aerosol Sci Technol.* 39, 1143-1163, 2005.

1002 Huneus, N., M. Schulz, Y. Balkanski, J. Griesfeller, S. Kinne, J. Prospero, S. Bauer, O. Boucher, M. Chin,  
1003 F. Dentener, T. Diehl, R. Easter, D. Fillmore, S. Ghan, P. Ginoux, A. Grini, L. Horowitz, D. Koch,  
1004 M.C. Krol, W. Landing, X. Liu, N. Mahowald, R.L. Miller, J.-J. Morcrette, G. Myhre, J.E. Penner, J.P.  
1005 Perlwitz, P. Stier, T. Takemura, and C. Zender, 2011: Global dust model intercomparison in AeroCom  
1006 phase I. *Atmos. Chem. Phys.*, 11, 7781-7816, doi:10.5194/acp-11-7781-2011.

1007 IPCC: (Intergovernmental Panel on Climate Change): The physical science basis. Contribution of working  
1008 group I to the fifth assessment report of the intergovernmental panel on climate change. T.F. Stocker, D.  
1009 Qin, G.-K. Plattner, M. Tignor, S.K. Allen, J. Boschung, A. Nauels, Y. Xia, V. Bex, and P.M. Midgley  
1010 (eds.). Cambridge University Press, Cambridge, United Kingdom and New York, NY, USA, 2013.  
1011 2013.

1012 Jimenez, J. L., Canagaratna, M. R., Donahue, N. M., Prevot, A. S. H., Zhang, Q., Kroll, J. H., DeCarlo, P.  
1013 F., Allan, J. D., Coe, H., Ng, N. L., Aiken, A. C., Docherty, K. S., Ulbrich, I. M.,  
1014 Jacob, D. J., Crawford, J. H., Maring, H., Clarke, A. D., Dibb, J. E., Emmons, L. K., Ferrare, R. A.,  
1015 Hostetler, C. A., Russell, P. B., Singh, H. B., Thompson, A. M., Shaw, G. E., McCauley, E., Pederson,  
1016 J. R., and Fisher, J. A.: The Arctic Research of the Composition of the Troposphere from Aircraft and  
1017 Satellites (ARCTAS) mission: design, execution, and first results, *Atmos. Chem. Phys.*, 10, 5191–  
1018 5212, doi:10.5194/acp-10-5191-2010, 2010.

1019 Jöckel, P., Kerkweg, A., Pozzer, A., Sander, R., Tost, H., Riede, H., Baumgaertner, A., Gromov, S., and  
1020 Kern, B.: Development cycle 2 of the Modular Earth Submodel System (MESSy2), *Geosci. Model  
1021 Dev.*, 3, 717-752, <https://doi.org/10.5194/gmd-3-717-2010>, 2010.

1022 Janssens-Maenhout, G., Crippa, M., Guizzardi, D., Dentener, F., Muntean, M., Pouliot, G., Keating, T.,  
1023 Zhang, Q., Kurokawa, J., Wankmüller, R., Denier van der Gon, H., Kuenen, J. J. P., Klimont, Z., Frost,  
1024 G., Darras, S., Koffi, B., and Li, M.: HTAP\_v2.2: a mosaic of regional and global emission grid maps

1025 for 2008 and 2010 to study hemispheric transport of air pollution, *Atmos. Chem. Phys.*, 15, 11411-  
1026 11432, doi:10.5194/acp-15-11411-2015, 2015

1027 Jöckel, P., Kerkweg, A., Pozzer, A., Sander, R., Tost, H., Riede, H., Baumgaertner, A., Gromov, S., and  
1028 Kern, B.: Development cycle 2 of the Modular Earth Submodel System (MESSy2), *Geosci. Model*  
1029 *Dev.*, 3, 717–752, doi:10.5194/gmd-3-717-2010, 2010.

1030 John, W., S. M. Wall, J. L. Ondo, and W. Winklmayr (1989), Acidic-aerosol size distributions during  
1031 SCAQS (Southern California Air Quality Study), final report, Rep. CA/DOH/AIHL/SP-51, Calif. Air  
1032 Resour. Board, Sacramento.

1033 Kanakidou, M., R.A. Duce, J.M. Prospero, A.R. Baker, C. Benitez-Nelson, F.J. Dentener, K.A. Hunter,  
1034 P.S. Liss, N. Mahowald, G.S. Okin, M. Sarin, K. Tsigaridis, M. Uematsu, L.M. Zamora, and T. Zhu,  
1035 2012: Atmospheric fluxes of organic N and P to the global ocean. *Glob. Biogeochem. Cycles*, 26,  
1036 GB3026, doi:10.1029/2011GB004277.

1037 Kanakidou, M., S. Myriokefalitakis, N. Daskalakis, G. Fanourgakis, A. Nenes, A. Baker, K. Tsigaridis, and  
1038 N. Mihalopoulos, 2016: Past, present and future atmospheric nitrogen deposition. *J. Atmos. Sci.*, 73,  
1039 no. 5, 2039-2047, doi:10.1175/JAS-D-15-0278.1.

1040 Karydis, V. A., Tsimpidi, A. P., Fountoukis, C., Nenes, A., Zavala, M., Lei, W., Molina, L. T., and Pandis,  
1041 S. N.: Simulating the fine and coarse inorganic particulate matter concentrations in a polluted  
1042 megacity, *Atmospheric Environment*, 44, 608-620, 2010.

1043 Karydis, V. A., Tsimpidi, A. P., Lei, W., Molina, L. T., and Pandis, S. N.: Formation of semivolatile  
1044 inorganic aerosols in the Mexico City Metropolitan Area during the MILAGRO campaign,  
1045 *Atmospheric Chemistry and Physics*, 11, 13305-13323, 2011.

1046 Karydis, V. A., A. P. Tsimpidi, A. Pozzer, M. Astitha, and J. Lelieveld, 2016: Effects of mineral dust on  
1047 global atmospheric nitrate concentrations. *Atmos. Chem. Phys.*, 16, 1491–1509, doi:10.5194/acp-16-  
1048 1491-2016.

1049 Kim, Y. P., Seinfeld, J. H., and Saxena, P.: Atmospheric gas–aerosol equilibrium I. Thermodynamic model,  
1050 *Aerosol Sci. Technol.*, 19, 157–181, 1993.

1051 Kim, D., M. Chin, H. Yu, T. Diehl, Q. Tan, R.A. Kahn, K. Tsigaridis, S.E. Bauer, T. Takemura, L. Pozzoli,  
1052 N. Bellouin, M. Schulz, S. Peyridieu, A. Chédin, and B. Koffi, 2014: Sources, sinks, and transatlantic  
1053 transport of North African dust aerosol: A multi-model analysis and comparison with remote-sensing  
1054 data. *J. Geophys. Res. Atmos.*, 119, no. 10, 6259-6277, doi:10.1002/2013JD021099.

1055 Kinne, S., Schulz, M., Textor, C., Guibert, S., Balkanski, Y., Bauer, S. E., Berntsen, T., Berglen, T. F.,  
1056 Boucher, O., Chin, M., Collins, W., Dentener, F., Diehl, T., Easter, R., Feichter, J., Fillmore, D., Ghan,  
1057 S., Ginoux, P., Gong, S., Grini, A., Hendricks, J., Herzog, M., Horowitz, L., Isaksen, I., Iversen, T.,  
1058 Kirkevåg, A., Kloster, S., Koch, D., Kristjansson, J. E., Krol, M., Lauer, A., Lamarque, J. F., Lesins,  
1059 G., Liu, X., Lohmann, U., Montanaro, V., Myhre, G., Penner, J., Pitari, G., Reddy, S., Seland, O.,  
1060 Stier, P., Takemura, T., and Tie, X.: An AeroCom initial assessment – optical properties in aerosol  
1061 component modules of global models, *Atmos. Chem. Phys.*, 6, 1815–1834, doi:10.5194/acp-6-1815-  
1062 2006, 2006.

1063 Koch, D., M. Schulz, S. Kinne, C. McNaughton, J.R. Spackman, T.C. Bond, Y. Balkanski, S. Bauer, T.  
1064 Berntsen, O. Boucher, M. Chin, A. Clarke, N. De Luca, F. Dentener, T. Diehl, O. Dubovik, R. Easter,  
1065 D.W. Fahey, J. Feichter, D. Fillmore, S. Freitag, S. Ghan, P. Ginoux, S. Gong, L. Horowitz, T. Iversen,  
1066 A. Kirkevåg, Z. Klimont, Y. Kondo, M. Krol, X. Liu, R.L. Miller, V. Montanaro, N. Moteki, G.  
1067 Myhre, J.E. Penner, J.P. Perlwitz, G. Pitari, S. Reddy, L. Sahu, H. Sakamoto, G. Schuster, J.P.  
1068 Schwarz, Ø. Seland, P. Stier, N. Takegawa, T. Takemura, C. Textor, J.A. van Aardenne, and Y. Zhao,  
1069 2009: Evaluation of black carbon estimations in global aerosol models. *Atmos. Chem. Phys.*, 9, 9001-  
1070 9026, doi:10.5194/acp-9-9001-2009.

1071 Kinnison, D. E., P. S. Connell, J. Rodriguez, D. B. Considine, D. A. Rotman, J. Tannahill, R. Ramarosan,  
1072 A. Douglass, S. Baughcum, L. Coy, P. Rasch, D. Waugh, 2001: The Global Modeling Initiative  
1073 assessment model: Application to high-speed civil transport perturbation, *J. Geophys. Res.*, 106, 1693-  
1074 1712.

1075 Lacis, A. A., Refractive Indices of Three Hygroscopic Aerosols and their Dependence on Relative  
1076 Humidity, [http://gacp.giss.nasa.gov/data\\_sets/lacis/introduction.pdf](http://gacp.giss.nasa.gov/data_sets/lacis/introduction.pdf).

1077 Lamarque, J.-F., J. T. Kiehl, G. P. Brasseur, T. Butler, P. Cameron-Smith, et al. (2005), Assessing future  
1078 nitrogen deposition and carbon cycle feedback using a multimodel approach : Analysis of nitrogen  
1079 deposition, *J. of Geophys. Res.*, Vol. 110, D19303, doi: 10.1029/2005JD005825.

1080 Lee, T., X.-Y. Yu, B. Ayres, S. M. Kreidenweis, W. C. Malm, J. L. Collett Jr., Observations of fine and  
1081 coarse particle nitrate at several rural locations in the United States, *Atmospheric Environment* 42,  
1082 2720–2732, 2008.

1083 Li, J., W.-C. Wang, H. Liao, and W. Chang. 2014. Past and future direct radiative forcing of nitrate aerosol  
1084 in East Asia. *Theor. Appl. Climatol.* 1–14. doi:10.1007/s00704-014-1249-1.

1085 Liao, H., P. J. Adams, S. H. Chung, J. H. Seinfeld, L. J. Mickley, and D. J. Jacob (2003), Interactions  
1086 between tropospheric chemistry and aerosols in a unified general circulation model, *J. Geophys. Res.*,  
1087 108(D1), 4001, doi:10.1029/2001JD001260.

1088 Liu, X., J. E. Penner, S. J. Ghan, and M. Wang, 2007: Inclusion of Ice Microphysics in the NCAR  
1089 Community Atmospheric Model Version 3 (CAM3). *J. Climate*, 20, 4526-4547.

1090 Liu, Y., G. Gibson, C. Cain, H. Wang, G. Grassian, and A. Laskin (2008) Kinetics of Heterogeneous  
1091 Reaction of CaCO<sub>3</sub> Particles with Gaseous HNO<sub>3</sub> over a Wide Range of Humidity, *J. Physical  
1092 Chemistry A*, doi:10.1021/jp076169h

1093 Malm, W. C., Schichtel, B. A., Pitchford, M. L., Ashbaugh, L. L., and Eldred, R. A.: Spatial and monthly  
1094 trends in speciated fine particle concentration in the United States, *J. Geophys. Res. Atmos.*, 109(D3),  
1095 D03306, doi:10.1029/2003JD003739, 2004.

1096 Metzger, S., F. Dentener, S. Pandis, and J. Lelieveld (2002), Gas/aerosol partitioning: 1. A computationally  
1097 efficient model, *J. of Geophys. Res.* Vol. 107, No. D16, 4312, 10.1029/2001JD001102.

1098 Mezuman, K., S.E. Bauer, and K. Tsigaridis, 2016: Evaluating secondary inorganic aerosols in three  
1099 dimensions. *Atmos. Chem. Phys.*, 16, 10651-10669, doi:10.5194/acp-16-10651-2016.

1100 Milegroet, H. Van and D. W. Cole, The Impact of Nitrification on Soil Acidification and Cation Leaching  
1101 in a Red Alder Ecosystem, ACSESS, Alliance of Crop, Soil, and Environmental Science Societies,  
1102 doi:10.2134/jeq1984.00472425001300040015x ,1984

1103 Myhre, G., A. Grini, and S. Metzger (2006), Modeling of nitrate and ammonium-containing aerosols  
1104 in presence of sea salt, *Atmos. Chem. Phys.*, 6, 4809-4821, [www.atmos-chem-phys.net/6/4809/2006/](http://www.atmos-chem-phys.net/6/4809/2006/).

1105 Myhre, G., B. H. Samset, M. Schulz, Y. Balkanski, S. Bauer, T. K. Berntsen, H. Bian, N. Bellouin, M.  
1106 Chin, T. Diehl, R. C. Easter, J. Feichter, S. J. Ghan, D. Hauglustaine, T. Iversen, S. Kinne, A.  
1107 Kirkevåg, J.-F. Lamarque, G. Lin, X. Liu, G. Luo, X. Ma, J. E. Penner, P. J. Rasch, Ø. Seland, R. B.  
1108 Skeie, P. Stier, T. Takemura, K. Tsigaridis, Z. Wang, L. Xu, H. Yu, F. Yu, J.-H. Yoon, K. Zhang, H.  
1109 Zhang, and C. Zhou, Radiative forcing of the direct aerosol effect from AeroCom Phase II simulations,  
1110 *Atmos. Chem. Phys.*, 13, 1853-1877, doi:10.5194/acp-13-1853-2013, 2013.

1111 Nowak, J., J. B., Weinheimer, A. J., Hoff, R. M., Berkoff, T. A., Beyersdorf, A. J., Olson, J., Crawford, J.  
1112 H., and Cohen, R. C.: On the effectiveness of nitrogen oxide reductions as a control over ammonium  
1113 nitrate aerosol, *Atmos. Chem. Phys.*, 16, 2575–2596, doi:10.5194/acp-16-2575-2016, 2016

1114 Paulot, F., Ginoux, P., Cooke, W. F., Donner, L. J., Fan, S., Lin, M.-Y., Mao, J., Naik, V., and Horowitz, L.  
1115 W.: Sensitivity of nitrate aerosols to ammonia emissions and to nitrate chemistry: implications for  
1116 present and future nitrate optical depth, *Atmos. Chem. Phys.*, 16, 1459–1477, doi:10.5194/acp-16-  
1117 1459-2016, <http://www.atmos-chem-phys.net/16/1459/2016/>, 2016.

1118 Phoenix, G., W. K. Hicks, S. Cinderby, J. C. I. Kuylenstierna, W. D. Stock, et al. (2006), Atmospheric  
1119 nitrogen deposition in world biodiversity hotspots: the need for a greater global perspective in  
1120 assessing N deposition impacts, *Global Change Biology*, 12, 470-476, doi: 10.1111/j.1365-  
1121 2486.2006.01104.x.

1122 Prentice, M. J., et al. (2001), The carbon cycle and atmospheric carbon dioxide, in *Climate Change 2001*,  
1123 pp. 184-237, Cambridge Univ. Press, New York.

1124 Pringle, K. J., Tost, H., Message, S., Steil, B., Giannadaki, D., Nenes, A., Fountoukis, C., Stier, P., Vignati,  
1125 E., and Lelieveld, J.: Description and evaluation of GMXe: a new aerosol submodel for global  
1126 simulations (v1), *Geoscientific Model Development*, 3, 391-412, 2010.

1127 Pusede, S. E., Duffey, K. C., Shusterman, A. A., Saleh, A., Laughner, J. L., Wooldridge, P. J., Zhang, Q.,  
1128 Parworth, C. L., Kim, H., Capps, S. L., Valin, L. C., Cappa, C. D., Fried, A., Walega, Riemer, N., H.  
1129 Vogel, B. Vogel, B. Schell, I. Ackermann, C. Kessler, and H. Hass (2003), Impact of the  
1130 heterogeneous hydrolysis of N<sub>2</sub>O<sub>5</sub> on chemistry and nitrate aerosol formation in the lower troposphere  
1131 under photochemical conditions, *J. Geophys. Res.*, 108(D4), 4144, doi:10.1029/2002JD002436.

1132 Sander, S. P., J. Abbatt, J. R. Barker, J. B. Burkholder, R. R. Friedl, D. M. Golden, R. E. Huie, C. E. Kolb,  
1133 M. J. Kurylo, G. K. Moortgat, V. L. Orkin and P. H. Wine "Chemical Kinetics and Photochemical  
1134 Data for Use in Atmospheric Studies, Evaluation No. 17," JPL Publication 10-6, Jet Propulsion  
1135 Laboratory, Pasadena, 2011 <http://jpldataeval.jpl.nasa.gov>.



1136 Saxena, P., Hudischeyskyj, A. B., Seigneur, C., and Seinfeld, J. H., A comparative study of  
1137 equilibrium approaches to the chemical characterization of secondary aerosols, *Atmos. Environ.*  
1138 20:1471- 1483, 1986.

1139 Schaap, M., Müller, K., & Ten Brink, H. M. (2002). Constructing the European aerosol nitrate  
1140 concentration field from quality analysed data. *Atmospheric Environment*, 36(8), 1323-1335.

1141 Schaap, M., van Loon, M., ten Brink, H. M., Dentener, F. J., and Builtjes, P. J. H.: Secondary  
1142 inorganic aerosol simulations for Europe with special attention to nitrate, *Atmos. Chem. Phys.*, 4,  
1143 857-874, doi:10.5194/acp-4-857-2004, 2004.

1144 Schmidt, G.A., M. Kelley, L. Nazarenko, R. Ruedy, G.L. Russell, I. Aleinov, M. Bauer, S.E. Bauer,  
1145 M.K. Bhat, R. Bleck, V. Canuto, Y.-H. Chen, Y. Cheng, T.L. Clune, A. Del Genio, R. de  
1146 Fainchtein, G. Faluvegi, J.E. Hansen, R.J. Healy, N.Y. Kiang, D. Koch, A.A. Lacis, A.N.  
1147 LeGrande, J. Lerner, K.K. Lo, E.E. Matthews, S. Menon, R.L. Miller, V. Oinas, A.O. Oloso, J.P.  
1148 Perlwitz, M.J. Puma, W.M. Putman, D. Rind, A. Romanou, M. Sato, D.T. Shindell, S. Sun, R.A.  
1149 Syed, N. Tausnev, K. Tsigaridis, N. Unger, A. Voulgarakis, M.-S. Yao, and J. Zhang, 2014:  
1150 Configuration and assessment of the GISS ModelE2 contributions to the CMIP5 archive. *J. Adv.*  
1151 *Model. Earth Syst.*, 6, no. 1, 141-184, doi:10.1002/2013MS000265.

1152 Schulz, M., Textor, C., Kinne, S., Balkanski, Y., Bauer, S., Berntsen, T., Berglen, T., Boucher, O.,  
1153 Dentener, F., Guibert, S., Isaksen, I. S. A., Iversen, T., Koch, D., Kirkevåg, A., Liu, X.,  
1154 Montanaro, V., Myhre, G., Penner, J. E., Pitari, G., Reddy, S., Seland, Ø., Stier, P., and  
1155 Takemura, T.: Radiative forcing by aerosols as derived from the AeroCom present-day and pre-  
1156 industrial simulations, *Atmos. Chem. Phys.*, 6, 5225–5246, doi:10.5194/acp-6-5225-2006, 2006.

1157 Schutgens, N. A. J., Gryspeerdt, E., Weigum, N., Tsyro, S., Goto, D., Schulz, M. and Stier, P.: Will a  
1158 perfect model agree with perfect observations? The impact of spatial sampling, *Atmos. Chem.*  
1159 *Phys.*, 16(10), 6335-6353, 2016.

1160 Shindell, D. T., Faluvegi, G., and Bell, N.: Preindustrial-to-present-day radiative forcing by  
1161 tropospheric ozone from improved simulations with the GISS chemistry-climate GCM, *Atmos.*  
1162 *Chem. Phys.*, 3, 1675–1702, 2003.

1163 Silvern, R. F., Jacob, D. J., Kim, P. S., Marais, E. A., Turner, J. R., Campuzano-Jost, P., and  
1164 Jimenez, J. L.: Inconsistency of ammonium–sulfate aerosol ratios with thermodynamic  
1165 models in the eastern US: a possible role of organic aerosol, *Atmos. Chem. Phys.*, 17, 5107-  
1166 5118, 10.5194/acp-17-5107-2017, 2017.

1167 Simpson, D., Benedictow, A., Berge, H., Bergström, R., Emberson, L. D., Fagerli, H., Flechard, C. R.,  
1168 Hayman, G. D., Gauss, M., Jonson, J. E., Jenkin, M. E., Nyíri, A., Richter, C., Semeena, V. S., Tsyro,  
1169 S., Tuovinen, J. P., Valdebenito, Á., and Wind, P.: The EMEP MSC-W chemical transport model -  
1170 technical description, *Atmos. Chem. Phys.*, 12, 7825-7865, 10.5194/acp-12-7825-2012, 2012.

1171 Song, C. H., and G. R. Carmichael, Gas-particle partitioning of nitric acid modulated by alkaline aerosol, *J.*  
1172 *Atmos. Chem.*, 40, 1–22, 2001.

1173 Søvde, O. A., Prather, M. J., Isaksen, I. S. A., Berntsen, T. K., Stordal, F., Zhu, X., Holmes, C. D., and Hsu,  
1174 J.: The chemical transport model Oslo CTM3, *Geosci. Model Dev.*, 5, 1441-1469,  
1175 <https://doi.org/10.5194/gmd-5-1441-2012>, 2012.

1176 Strahan, S. E., Duncan, B. N., and Hoor, P.: Observationally derived transport diagnostics for the  
1177 lowermost stratosphere and their application to the GMI chemistry and transport model, *Atmos. Chem.*  
1178 *Phys.*, 7, 2435-2445, doi:10.5194/acp-7-2435-2007, 2007.

1179 Sudo, K., M. Takahashi, J. Kurokawa, and H. Akimoto, CHASER: A global chemical model of the  
1180 troposphere, 1. Model description, *J. Geophys. Res.*, 107(D17), 4339, doi:10.1029/2001JD001113,  
1181 2002.

1182 Takiguchi, Y., A. Takami, Y. Sadanaga, X. Lun, A. Shimizu, I. Matsui, N. Sugimoto, W. Wang, H.  
1183 Bandow, and S. Hatakeyama (2008), Transport and transformation of total reactive nitrogen over the  
1184 East China Sea, *J. Geophys. Res.*, 113, D10306, doi:10.1029/2007JD009462.

1185 Textor, C., Schulz, M., Guibert, S., Kinne, S., Balkanski, Y., Bauer, S., Berntsen, T., Berglen, T., Boucher,  
1186 O., Chin, M., Dentener, F., Diehl, T., Easter, R., Feichter, H., Fillmore, D., Ghan, S., Ginoux, P.,  
1187 Gong, S., Grini, A., Hendricks, J., Horowitz, L., Huang, P., Isaksen, I., Iversen, I., Kloster, S., Koch,  
1188 D., Kirkevåg, A., Kristjansson, J. E., Krol, M., Lauer, A., Lamarque, J. F., Liu, X., Montanaro, V.,  
1189 Myhre, G., Penner, J., Pitari, G., Reddy, S., Seland, Ø., Stier, P., Takemura, T., and Tie, X.: Analysis

1190 and quantification of the diversities of aerosol life cycles within AeroCom, *Atmos. Chem. Phys.*, 6,  
1191 1777–1813, doi:10.5194/acp-6-1777-2006, 2006.

1192 Tost, H., Jöckel, P., Kerkweg, A., Sander, R., and Lelieveld, J.: Technical note: A new comprehensive  
1193 SCAVenging submodel for global atmospheric chemistry modelling, *Atmos. Chem. Phys.*, 6, 565-574,  
1194 doi:10.5194/acp-6-565-2006, 2006.

1195 Trail, M., Tsimpidi, A. P., Liu, P., Tsigaridis, K., Rudokas, J., Miller, P., Nenes, A., Hu, Y., and Russell, A.  
1196 G.: Sensitivity of air quality to potential future climate change and emissions in the United States and  
1197 major cities, *Atmospheric Environment*, 94, 552-563, 2014.

1198 Trumpf, E. R., Fountoukis, C., Donahue, N. M., and Pandis, S. N.: Improvement of simulation of fine  
1199 inorganic PM levels through better descriptions of coarse particle chemistry, *Atmospheric  
1200 Environment*, 102, 274-281, 2015.

1201 Tsigaridis, K., Daskalakis, N., Kanakidou, M., Adams, P. J., Artaxo, P., Bahadur, R., Balkanski, Y.,  
1202 Bauer, S. E., Bellouin, N., Benedetti, A., Bergman, T., Berntsen, T. K., Beukes, J. P., Bian, H.,  
1203 Carslaw, K. S., Chin, M., Curci, G., Diehl, T., Easter, R. C., Ghan, S. J., Gong, S. L., Hodzic, A.,  
1204 Hoyle, C. R., Iversen, T., Jathar, S., Jimenez, J. L., Kaiser, J. W., Kirkevåg, A., Koch, D., Kokkola, H.,  
1205 Lee, Y. H., Lin, G., Liu, X., Luo, G., Ma, X., Mann, G. W., Mihalopoulos, N., Morcrette, J.-J.,  
1206 Müller, J.-F., Myhre, G., Myriokefalitakis, S., Ng, N. L., O'Donnell, D., Penner, J. E., Pozzoli, L.,  
1207 Pringle, K. J., Russell, L. M., Schulz, M., Sciare, J., Seland, Ø., Shindell, D. T., Sillman, S.,  
1208 Skeie, R. B., Spracklen, D., Stavrou, T., Steenrod, S. D., Takemura, T., Tiitta, P., Tilmes, S.,  
1209 Tost, H., van Noije, T., van Zyl, P. G., von Salzen, K., Yu, F., Wang, Z., Wang, Z., Zaveri, R. A.,  
1210 Zhang, H., Zhang, K., Zhang, Q., and Zhang, X.: The AeroCom evaluation and intercomparison of  
1211 organic aerosol in global models, *Atmos. Chem. Phys.*, 14, 10845-10895, doi:10.5194/acp-14-10845-  
1212 2014, 2014.

1213 Tsimpidi, A. P., Karydis, V. A., and Pandis, S. N.: Response of inorganic fine particulate matter to  
1214 emission changes of sulfur dioxide and ammonia: The eastern United States as a case study, *Journal of  
1215 the Air & Waste Management Association*, 57, 1489-1498, 2007.

1216 Tsimpidi, A. P., Karydis, V. A., and Pandis, S. N.: Response of Fine Particulate Matter to Emission  
1217 Changes of Oxides of Nitrogen and-Anthropogenic Volatile Organic Compounds in the Eastern United  
1218 States, *Journal of the Air & Waste Management Association*, 58, 1463-1473, 2008.

1219 Vieno, M., Heal, M. R., Twigg, M. M., MacKenzie, I. A., Braban, C. F., Lingard, J. J. N. Ritchie, S., Beck,  
1220 R. C., A., M., Ots, R., DiMarco, C. F., Nemitz, E., Sutton, M. A., and Reis, S.: The UK particulate  
1221 matter air pollution episode of March-April 2014: more than Saharan dust., *Environ. Res. Lett.*,  
1222 doi:10.1088/1748-9326/11/4/044004, 2016.

1223 Walker, J. M., Philip, S., Martin, R. V., and Seinfeld, J. H.: Simulation of nitrate, sulfate, and ammonium  
1224 aerosols over the United States, *Atmos. Chem. Phys.*, 12, 11213–11227, doi:10.5194/acp-12-11213-  
1225 2012, 2012.

1226 Watanabe, S., T. Hajima, K. Sudo, T. Nagashima, T. Takemura, H. Okajima, *et al.* MIROC-ESM 2010:  
1227 model description and basic results of CMIP5-20c3m experiments, *Geosci. Model Dev.*, 4 (2011), pp.  
1228 845–872.

1229 Weber, R. J., Guo, H., Russell, A. G., and Nenes, A.: High aerosol acidity despite declining  
1230 atmospheric sulfate concentrations over the past 15 years, *Nature Geosci.*, 9, 282-285,  
1231 10.1038/ngeo2665, 2016.

1232 Williams, E. J., S. T. Sandholm, J. D. Bradshaw, J. S. Schendel, A. O. Langford, P. K. Quinn, P. J. LeBel,  
1233 S. A. Vay, P. D. Roberts, R. B. Norton, B. A. Watkins, M. P. Buhr, D. D. Parrish, J. G. Calvert, and F.  
1234 C. Fehsenfeld, An intercomparison of five ammonia measurement techniques, *J. Geophys. Res.*, Vol.,  
1235 97, No. D11, Pages 11591-11611, July 20, 1992.

1236 van der Werf, G. R., Randerson, J. T., Giglio, L., Collatz, G. J., Mu, M., Kasibhatla, P. S., Morton, D. C.,  
1237 DeFries, R. S., Jin, Y., and van Leeuwen, T. T.: Global fire emissions and the contribution of  
1238 deforestation, savanna, forest, agricultural, and peat fires (1997–2009), *Atmos. Chem. Phys.*, 10,  
1239 11707-11735, doi:10.5194/acp-10-11707-2010, 2010.

1240 Zender, C. S., Bian, H. S., and Newman, D.: Mineral Dust Entrainment and Deposition (DEAD) model:  
1241 Description and 1990s dust climatology, *J. Geophys. Res.-Atmos.*, 108, 4416,  
1242 doi:10.1029/2002jd002775, 2003.

1243 Zhou, J., B. Gu, W. H. Schlesinger, X. Ju, Significant accumulation of nitrate in Chinese semi-humid  
1244 croplands, *Scientific Reports* 6, Article number: 25088, doi:10.1038/srep25088, 2016.

**Table 1. Nitrate chemical mechanism and physical properties of AeroCom models**

Model	CHEM-EQM	HNO <sub>3</sub> chem mechanism	N <sub>2</sub> O <sub>5</sub> Hydrolysis	CHEM DUST	CHEM SEASALT	How do CHEMDUSS <sup>a</sup>	Bins for nitrate	Model Name & resolution	References
CHASER	ISORROPIA-I	CHASER (Sudo et al., 2002)	$\gamma^b$ (0.1 for SO <sub>4</sub> <sup>2-</sup> , NO <sub>3</sub> <sup>-</sup> , OC, DU, and SS, and 0.05 for liquid cloud particles) (Dentener and Crutzen, 1993)	No	No	---	Fine mode	MIROC, GCM, 2.8°x2.8°x64	Watanabe et al., 2011
EMAC	ISORROPIA-II (Stable state <sup>c</sup> )	MESSy2 (Jöckel et al., 2010)	$\gamma$ (STA), STA <sup>d</sup> : climatological aerosol in Aitken, accumulation, and coarse soluble modes (Jöckel et al 2010).	Yes	Yes	ISORROPIA-II (TEQM)	4 bins: Nucleation, Aitken, Accumulation, Coarse	ECHAM5, GCM, 2.8°x2.8°x31	Karydis et al., 2016
EMEP	MARS	EMEP EmChem09 (Simpson et al., 2012)	$\gamma$ (STA, T, RH), STA: NH <sub>4</sub> <sup>+</sup> , SO <sub>4</sub> <sup>2-</sup> , NO <sub>3</sub> <sup>-</sup> (Evans and Jacob, 2005; Davis et al., 2008)	Yes	Yes	First order loss (HETCHEM)	Fine and coarse	ECMWF-IFS, CTM, 0.5x0.5°x20	Simpson et al., 2012
GMI	RPMARES (Stable state)	GMI (Straham et al., 2007)	$\gamma$ (STA, T, RH), STA: BC, OC, SO <sub>4</sub> <sup>2-</sup> , DU, SS (Evans and Jacob, 2005).	Yes	Yes	first order loss (HETCHEM)	3 bins: (D<0.1, 0.1 – 2.5, > 2.5 $\mu$ m)	MERRA2, CTM, 2.5°x2°x72	Bian et al., 2009
INCA	INCA (Stable state)	INCA tropospheric chemistry (Hauglustaine et al., 2004)	$\gamma$ (STA, T, RH), STA: BC, SO <sub>4</sub> <sup>2-</sup> , DU, SS (Evans and Jacob, 2005).	Yes	Yes	first order loss (HETCHEM)	2 bins : (D< 1 $\mu$ m and 1 - 10 $\mu$ m)	LMD-v4, GCM, 1.9°x3.75°x39	Hauglustaine et al., 2014
GISS MATRIX	ISORROPIA-II (Stable state)	MATRIX Bauer (2008) and tropospheric chemistry (Shindell et al., 2003)	$\gamma$ (STA), STA: SO <sub>4</sub> <sup>2-</sup> (Dentener and Crutzen, 1993)	No	No	NO	Distributed over all mixing states e.g. size distributions.	NASA GISS-E2, GCM, 2°x2.5°x40	Schmidt et al 2014
GISS OMA	EQSAM_v03d (Metastable <sup>e</sup> )	OMA (Bauer 2007) and tropospheric chemistry (Shindell et al., 2003)	$\gamma$ (STA), STA: SO <sub>4</sub> <sup>2-</sup> (Dentener and Crutzen, 1993)	Yes	No	Bauer and Koch, 2005 (HETCHEM)	Fine mode	NASA GISS-E2, GCM, 2°x2.5°x40	Schmidt et al 2014
Oslo CTM2	EQSAM_v03d (Metastable)	Oslo CTM2 (Berntsen and Isaksen, 1997)	$\gamma$ (STA), STA: climatology aerosol (Dentener and Crutzen, 1993; Søvde et al., 2012).	No	Yes	EQSAM_v03d (TEQM)	2 bins: fine and coarse mode	ECMWF, CTM, 2.8°x2.8°x60	Myhre et al., 2006
Oslo CTM3	EQSAM_v03d (Metastable)	Oslo CTM2 (Berntsen and Isaksen, 1997)	$\gamma$ (STA), STA: climatology aerosol (Dentener and Crutzen, 1993; Søvde et al., 2012).	No	Yes	EQSAM_v03d (TEQM)	2 bins: fine and coarse mode	ECMWF, CTM, 2.25°x2.25°x60	Myhre et al., 2006

<sup>a</sup>CHEMDUSS: Chemistry reaction on dust and sea salt particles

<sup>b</sup> $\gamma$ : the dimensionless uptake coefficient

<sup>c</sup>Stable state: where salts precipitate once the aqueous phase becomes saturated

<sup>d</sup>STA: Surface of Tropospheric Aerosols

<sup>e</sup>Metastable: where the aerosol is composed only of a supersaturated aqueous phase

1251

**Table 2. Characteristics of thermodynamic equilibrium models**

	ISORROPIA-I	ISORROPIA-II	MARS	RPMARES	INCA	EQSAM_v03d
Species	Sulfate, nitrate, ammonium, sodium, chloride	Sulfate, nitrate, ammonium, sodium, chloride, crustal species	Sulfate, nitrate, ammonium	Sulfate, nitrate, ammonium	Sulfate, nitrate, ammonium	Sulfate, nitrate, ammonium, sodium, chloride
# of components	23	34	16	11	9	18
# of reactions	15	27	7	6	4	25
Multicomponent activity coefficient	Bromley	Bromley	Bromley	Bromley	Seinfeld and Pandis	Metzger
Binary activity coefficient	Kusik and Meissner	Kusik and Meissner	Pitzer	Pitzer	Seinfeld and Pandis	Metzger
Water activity	ZSR <sup>a</sup>	ZSR	ZSR	ZSR		ZSR
Kelvin effect	No	No	No	No	No	No
Quantities that determine subdomains	[Na <sup>+</sup> ], [NH <sub>4</sub> <sup>+</sup> ], [SO <sub>4</sub> <sup>2-</sup> ]	[Ca <sup>2+</sup> ], [K <sup>+</sup> ], [Mg <sup>2+</sup> ], [Na <sup>+</sup> ], [NH <sub>4</sub> <sup>+</sup> ], [SO <sub>4</sub> <sup>2-</sup> ]	RH, [NH <sub>4</sub> <sup>+</sup> ], [SO <sub>4</sub> <sup>2-</sup> ]	[NH <sub>4</sub> <sup>+</sup> ], [SO <sub>4</sub> <sup>2-</sup> ]	[NH <sub>4</sub> <sup>+</sup> ], [SO <sub>4</sub> <sup>2-</sup> ]	[NH <sub>4</sub> <sup>+</sup> ], [SO <sub>4</sub> <sup>2-</sup> ]
# of subdomains	4	5	4	2	3	3

1252

<sup>a</sup>ZSR: Zdanovskii-Stokes-Robinson

1253

1254

**Table 3. Summary of the observational data used in this study**

SURFACE NETWORK	QUANTITY	COVER AREA	# of sites in 2008	SAMPLE FREQUENCY	SOURCE
CASTNET	Concentration of HNO <sub>3</sub> , NO <sub>3</sub> <sup>-</sup> , NH <sub>4</sub> <sup>+</sup> , SO <sub>4</sub> <sup>2-</sup>	North America	83	weekly	www.epa.gov/castnet/clearsession.do
	Dry deposition of them				
AMoN	Concentration of NH <sub>3</sub>	U.S.	19	2-weekly	http://nadp.isws.illinois.edu/
NADP/NTN	Wet deposition of HNO <sub>3</sub> +NO <sub>3</sub> <sup>-</sup> , NH <sub>4</sub> <sup>+</sup> , SO <sub>4</sub> <sup>2-</sup>	U.S.	253	weekly	nadp.isws.illinois.edu
EMEP	Concentration of HNO <sub>3</sub> , NH <sub>3</sub> , NO <sub>3</sub> <sup>-</sup> , NH <sub>4</sub> <sup>+</sup> , SO <sub>4</sub> <sup>2-</sup>	Europe	35	daily	http://www.nilu.no/projects/ccc/index.html
EANET	Concentration of HNO <sub>3</sub> , NH <sub>3</sub> , NO <sub>3</sub> <sup>-</sup> , NH <sub>4</sub> <sup>+</sup> , SO <sub>4</sub> <sup>2-</sup>	East Asia	56	Daily to 2-weekly	http://www.eanet.asia/eanet/brief.html
	Wet deposition of HNO <sub>3</sub> +NO <sub>3</sub> <sup>-</sup> , NH <sub>4</sub> <sup>+</sup> , SO <sub>4</sub> <sup>2-</sup>			24 hours or precipitation event	
AIRCRAFT CAMPAIGNS	QUANTITY	COVER AREA	# of Flights	CAMPAIGN PERIOD	SOURCE
ARCTAS-A	Concentration of NO <sub>3</sub> <sup>-</sup> , NH <sub>4</sub> <sup>+</sup> , SO <sub>4</sub> <sup>2-</sup>	Alaska, U.S.	11	March-April	http://www-air.larc.nasa.gov/cgi-bin/arcstat-c
ARCTAS-CARB		California Bay area U.S.	6	June	
ARCTAS-B		Central Canada	7	July	

1255

1256

**Table 4a. NO<sub>3</sub><sup>-</sup> global budget for each model**

Tracer	Model	Burden (Tg)	SConc (µg kg <sup>-1</sup> )	DDep (Tg a <sup>-1</sup> )	WDep (Tg a <sup>-1</sup> )	ChemDUSS (Tg a <sup>-1</sup> )	ChemP <sup>a</sup> (Tg a <sup>-1</sup> )	Lifetime (days)	AOD <sup>b</sup>
NO <sub>3</sub> <sup>-</sup>	CHASER	0.16	0.18	-	-	-	-	-	0.0076
	EMAC	0.67	0.47	46.3	-	-	-	-	-
	EMEP	0.96	0.30	15.0	62.7	(71.7) <sup>c</sup>	4.5	0.0073	-
	GISS-MATRIX	0.22	0.06	1.3	9.6	(10.9)	7.4	-	-
	GISS-OMA	0.14	0.05	1.1	5.5	(6.6)	7.8	0.0153	-
	GMI	0.26	0.22	14.9	31.5	41.9	4.8	2.1	0.0047

INCA	0.79	0.17	4.5	44.6	44.1	9.8	5.9	0.0064
Oslo-CTM2	0.60	0.25	47.8	61.5	(109.3)		2.0	0.0018
Oslo-CTM3	1.88	0.36	34.6	90.6	(125.2)		5.5	-
Avg	0.63	0.23	20.7	45.9		60.6	5.0	0.0072
Med	0.60	0.22	15.0	44.6		46.7	5.5	0.0064
Ratio <sup>d</sup>	13.4	9.4	43.5	16.5		19.0	3.9	8.5

- 1257 a: ChemP refers to NO<sub>3</sub><sup>-</sup> chemical production associated with NH<sub>3</sub>/NH<sub>4</sub><sup>+</sup>  
1258 b: AOD here includes NH<sub>4</sub><sup>+</sup> that is associated to NO<sub>3</sub><sup>-</sup> for all models except EMEP  
1259 c: value inside parenthesis is estimated total NO<sub>3</sub><sup>-</sup> chemical production based on its  
1260 total loss, while budget without parenthesis is reported directly by model.  
1261 d: a ratio between maximum to minimum model simulations  
1262  
1263

**Table 4b NH<sub>3</sub> and NH<sub>4</sub><sup>+</sup> global budget for each model**

Tracer	Model	Emi (Tg a <sup>-1</sup> )	Burden (Tg)	SConc (µg kg <sup>-1</sup> )	DDep (Tg a <sup>-1</sup> )	WDep (Tg a <sup>-1</sup> )	ChemP/L <sup>a</sup> (Tg a <sup>-1</sup> )	Lifetime (days)	AOD	
NH <sub>4</sub> <sup>+</sup>	CHASER		0.75	0.44	20.9	7.2	(28.1) <sup>b</sup>	9.8	-	
	EMAC		0.19	0.12	3.6	44.5 <sup>c</sup>	-	-	-	
	EMEP		0.20	0.15	4.0	26.4	(30.4)	2.4	0.0059	
	GISS-MATRIX		0.31	0.18	4.1	27.9	(32.0)	3.5	-	
	GISS-OMA		0.31	0.19	4.2	24.0	(28.2)	4.0	-	
	GMI		0.17	0.14	1.7	30.6	32.2	1.9	-	
	INCA		0.39	0.08	2.4	20.4	22.9	6.3	-	
	Oslo-CTM2		0.29	0.14	5.3	32.6	(37.9)	2.8	-	
	Oslo-CTM3		0.30	0.16	5.6	26.1	(31.7)	3.5	-	
	Avg			0.32	0.18	5.8	24.4 <sup>d</sup>	30.4	4.3	
	Med			0.30	0.15	4.1	26.3 <sup>d</sup>	31.1	3.5	
	Ratio			4.4	5.5	12.3	4.5 <sup>c</sup>	1.7	5.2	
	NH <sub>3</sub>	CHASER	62.8	0.13	0.46	19.8	6.8	(36.2) <sup>b</sup>	0.76	
EMAC		59.3	0.85	1.39	15.5	-	-	-		
EMEP		56.9	0.09	0.46	15.4	18.2	(33.6)	0.98		
GISS-MATRIX		63.4 <sup>e</sup>	0.17	0.26	18.1	13.4	(31.9)	0.98		
GISS-OMA		63.4 <sup>e</sup>	0.17	0.25	18.4	16.7	(28.3)	0.98		
GMI		60.4	0.11	0.40	12.6	17.5	30.4	0.67		
INCA		70.5 <sup>e</sup>	0.12	0.39	29.3	18.6	22.4	0.62		
Oslo-CTM2		65.9	0.08	0.27	15.8	8.1	(42.0)	0.44		
Oslo-CTM3		63.3	0.05	0.51	23.7	7.7	(31.9)	0.29		
Avg		62.9	0.20	0.49	18.7	13.4	32.1	0.72		
Med		63.3	0.12	0.40	18.1	15.1	31.9	0.72		
Ratio		1.2	17.0	5.6	2.3	2.7	1.9	3.4		

- 1264 <sup>a</sup>ChemP/L: chemical production or loss term  
1265 <sup>b</sup> chemical budgets inside parenthesis are inferred based on the reported emission  
1266 and total deposition  
1267 <sup>c</sup>EMAC gives total wet deposition of NH<sub>4</sub><sup>+</sup> and NH<sub>3</sub>  
1268 <sup>d</sup>Statistic values of NH<sub>4</sub><sup>+</sup> wet deposition do not include EMAC  
1269 <sup>e</sup> INCA uses ECLIPSE anthropogenic emissions, two GISS models use CMIP5  
1270 anthropogenic emission, and all other models use HTAPv2 anthropogenic emissions  
1271  
1272

1273 **Table 4c. HNO<sub>3</sub> global budget for each model**

Tracer	Model	Burden <sup>a</sup> (Tg)	SConc (µg kg <sup>-1</sup> )	DDep (Tg a <sup>-1</sup> )	WDep (Tg a <sup>-1</sup> )	CheAP <sup>b</sup> (Tg a <sup>-1</sup> )	CheGP <sup>c</sup> (Tg a <sup>-1</sup> )	CheAL <sup>d</sup> (Tg a <sup>-1</sup> )	CheGL <sup>e</sup> (Tg a <sup>-1</sup> )	Lifetime (days)
HNO <sub>3</sub>	CHASER	1.1	0.29	74.0 <sup>f</sup>	120.9 <sup>f</sup>	-	-	-	-	-
	EMAC	3.1	0.32	56.1	136.0 <sup>f</sup>	-	-	-	-	-
	EMEP	0.66	0.04	39.2	123.9	-	-	-	-	-
	GISS- MATRIX	5.7	0.12	61.7	167.5	-	-	-	-	-
	GISS- OMA	5.3	0.10	49.8	148.2	-	-	-	-	-
	GMI	1.8	0.18	39.7	128.1	128.1	413	42.6	299	3.5
	INCA	1.5	0.09	47.7	77.5	21	369	10.0	210	5.7
	Oslo- CTM2	1.3	0.05	36.1	66.0	-	-	-	-	-
	Oslo- CTM3	2.3	0.04	36.0	49.3	-	-	-	-	-
	Avg	2.5	0.14	45.8 <sup>g</sup>	108.7 <sup>g</sup>	-	-	-	-	-
	Med	1.8	0.10	43.7 <sup>g</sup>	123.9 <sup>g</sup>	-	-	-	-	-
Ratio	8.6	8.0	1.6 <sup>b</sup>	3.4 <sup>b</sup>	-	-	-	-	-	

1274 <sup>a</sup>HNO<sub>3</sub> burden for the atmosphere up to 100 hPa

1275 <sup>b</sup>CheAP: chemistry production from aerosol phase

1276 <sup>c</sup>CheGP: chemistry production from gas phase

1277 <sup>d</sup>CheAL: chemistry loss from aerosol phase

1278 <sup>e</sup>CheGL: chemistry loss from gas phase

1279 <sup>f</sup>for both HNO<sub>3</sub> and NO<sub>3</sub><sup>-</sup>

1280 <sup>g</sup>statistical values do not include CHASER and EMAC that report total dry or wet  
1281 deposition of HNO<sub>3</sub> and NO<sub>3</sub><sup>-</sup>

1282

1283 **Table 4d. SO<sub>4</sub><sup>2-</sup> global budget for each model**

Tracer	Model	Emi SO <sub>2</sub> (Tg a <sup>-1</sup> )	Emi SO <sub>4</sub> (Tg a <sup>-1</sup> )	Burden (Tg)	SConc (µg kg <sup>-1</sup> )	DDep (Tg a <sup>-1</sup> )	WDep (Tg a <sup>-1</sup> )	Chem GP <sup>a</sup> (Tg a <sup>-1</sup> )	Chem AqP <sup>b</sup> (Tg a <sup>-1</sup> )	Lifetime (days)	AOD
SO <sub>4</sub> <sup>2-</sup>	CHASER	111	0	3.3	1.44	22.1	137	(159)	(159)	7.6	0.0826
	EMAC	138	619 <sup>c</sup>	1.9	1.72	504 <sup>d</sup>	302	(187)	(187)	0.86	-
	EMEP	109	0	0.83	0.45	10.2	109	(119)	(119)	2.5	0.0232
	GISS- MATRIX	133	5.1	1.3	0.63	16.6	97	(109)	(109)	4.2	-
	GISS- OMA	133	5.1	1.1	0.53	11.8	112	52.7	66.2	3.3	0.0714
	GMI	111	0	1.1	0.58	7.5	205	126.5	86.1	3.6	0.0257
	INCA	116.	8.0	1.8	0.34	8.4	116	42.2	75.1	5.3	0.0417
	Oslo- CTM2	133	4.1	2.0	0.49	17.6	184	(198)	(198)	3.6	0.0366
	Oslo- CTM3	133	4.1	2.7	0.55	20.2	160	(176)	(176)	5.5	-
	Avg <sup>e</sup>	122		1.8	0.63	14.3	140		151	4.5	0.0469
	Med <sup>e</sup>	133		1.6	0.54	14.2	127		139	3.9	0.0392
Ratio <sup>e</sup>	1.2		4.0	4.2	2.9	2.1		2.0	3.0	3.6	

1284 <sup>a</sup> ChemGP: Chemistry production from gas phase reaction

1285 <sup>b</sup> ChemAqP: Chemistry production from aqueous phase reaction

1286 <sup>c</sup> EMAC emission also includes sea spray SO<sub>4</sub><sup>2-</sup>

1287 <sup>d</sup> EMAC dry deposition includes sedimentation and SO<sub>4</sub><sup>2-</sup> sedimentation is very high  
1288 since it has assumed that 7.7% of sea salt is SO<sub>4</sub><sup>2-</sup>

1289 <sup>d</sup> Statistical values do not include EMAC

1290

1291 **Table 5: Effective Henry Law constant used in the models**

<b>Aerocom Model</b>	<b>H<sup>0*</sup> (M/atm)</b>	<b>-ΔH<sub>sol</sub>/R (K)</b>
CHASER	3.0e+5	3400
EMAC <sup>a</sup>	-	-
EMEP <sup>b</sup>	-	-
GIS MATRIX	1.e+2	3415
GISS OMA	1.e+2	3415
GMI	1.05e6	4200
INCA	7.4e+1	3400
Oslo-CTM2	3.3e+6	0
Oslo-CTM3	3.3e+6	0

1292 <sup>a</sup>EMAC: See its wet deposition description in section 4.1.1.

1293 <sup>b</sup>EMEP: The model does not use Henry law but applies simple empirical scavenging  
 1294 ratio, which for NH<sub>3</sub> is 1.4e6 for in-cloud and 0.5e6 for below-cloud scavenging. The  
 1295 scavenging ratio by definition is the ratio the concentration of a certain pollutant in  
 1296 precipitation divided by the concentration of the pollutant in air.

1297

1298 **Table 6. Baseline and three sensitivity experiments in the GMI model**

<b>Experiment</b>	<b>Setup</b>	<b>Purpose</b>
<b>BASE</b>	Standard simulation as described in section 2.1	Baseline simulation
<b>TWET</b>	Set NH <sub>3</sub> effective Henry law constant from 1.05e+6 (pH= 5.0) to 62 (pure water)	Review impact of NH <sub>3</sub> wet deposition
<b>TnoNH3</b>	Turn off NO <sub>3</sub> <sup>-</sup> production from NH <sub>3</sub> /NH <sub>4</sub> <sup>+</sup>	Identify how large/where the NO <sub>3</sub> <sup>-</sup> formation from NH <sub>3</sub> /NH <sub>4</sub> <sup>+</sup>
<b>TnoHET</b>	Turn off NO <sub>3</sub> <sup>-</sup> production from dust and sea salt	Identify how large/where the NO <sub>3</sub> <sup>-</sup> formation from dust and sea salt

1299

1300 **Table 7: NO<sub>3</sub><sup>-</sup>, NH<sub>4</sub><sup>+</sup>, NH<sub>3</sub> and HNO<sub>3</sub> budgets from the base simulation and three**  
 1301 **sensitivity experiments**

<b>Tracer</b>	<b>Exps</b>	<b>Burden (Tg)</b>	<b>SConc (μg kg<sup>-1</sup>)</b>	<b>DDep (Tg a<sup>-1</sup>)</b>	<b>WDep (Tg a<sup>-1</sup>)</b>	<b>ChemDUSS (Tg a<sup>-1</sup>)</b>	<b>ChemP( Tg a<sup>-1</sup>)</b>	<b>Lifetime (days)</b>
NO <sub>3</sub> <sup>-</sup>	BASE	0.26	0.22	14.9	31.5	41.9	4.8	2.1
	Twet	0.97	0.23	14.8	43.3	41.0	18.3	6.0
	TnoNH3	0.20	0.17	14.7	27.5	42.3	0	1.7
	TnoHET	0.099	0.065	0.61	6.70	0	7.1	5.0

1302

<b>Tracer</b>	<b>Model</b>	<b>Emi (Tg a<sup>-1</sup>)</b>	<b>Burden (Tg)</b>	<b>SConc (μg kg<sup>-1</sup>)</b>	<b>DDep (Tg a<sup>-1</sup>)</b>	<b>WDep (Tg a<sup>-1</sup>)</b>	<b>ChemP/L (Tg a<sup>-1</sup>)</b>	<b>Lifetime (days)</b>
NH <sub>4</sub> <sup>+</sup>	BASE		0.17	0.14	1.7	30.6	32.2	1.9
	Twet		0.48	0.16	1.9	50.7	53.0	3.4
	TnoNH3		-	-	-	-	-	-
	TnoHET		0.17	0.14	1.6	30.6	32.2	1.9
NH <sub>3</sub>	BASE	60.4	0.11	0.40	12.6	17.5	30.4	0.67
	Twet		0.85	0.81	8.70	1.1	50.1	5.2
	TnoNH3		0.32	0.58	20.9	39.3	0	1.9
	TnoHET		0.10	0.40	12.6	17.4	30.4	1.2

1303

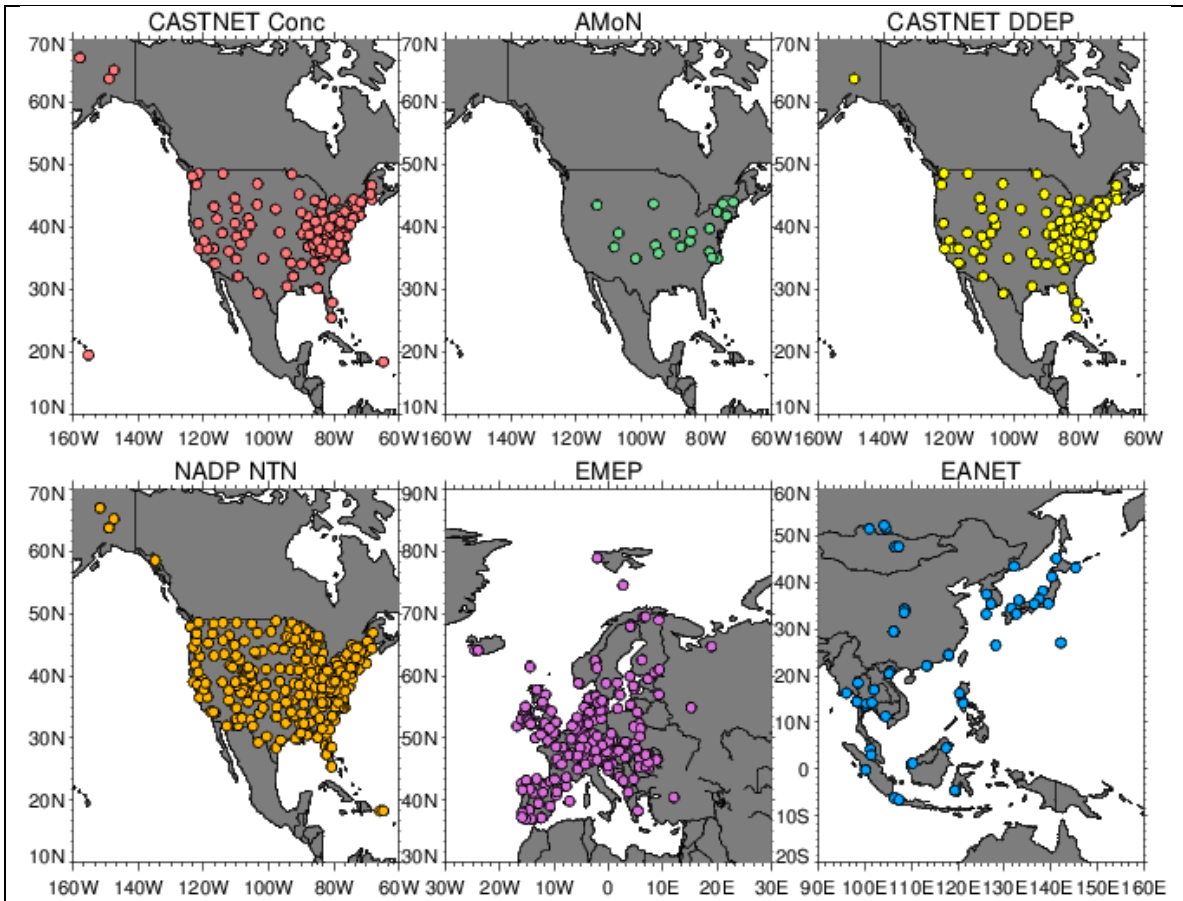


Figure 1. The observational station locations for CASTNET surface concentrations (CASTNET Conc), Ammonia surface monitor network over U.S. (AMON), CASTNET dry deposition (CASTNET DDEP); National Acid Deposition Network for wet deposition over U.S. (NADP NTN), surface concentrations over Europe (EMEP), and surface dry and wet deposition over Asia (EANET).

1304  
1305  
1306

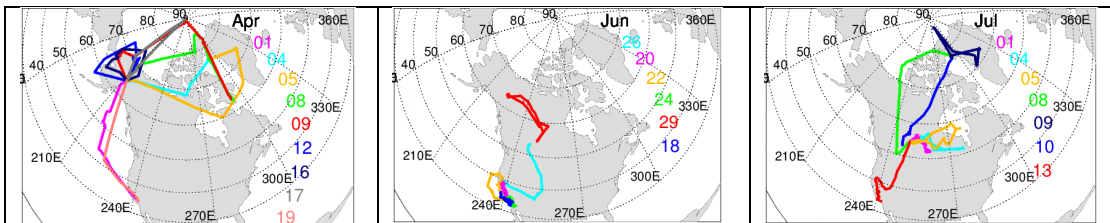


Figure 2. Flight-tracks of ARTCTA-A (left), ARCTAS-CARB (middle), and ARCTAS-B (right). The colors represent observations during different days.

1307



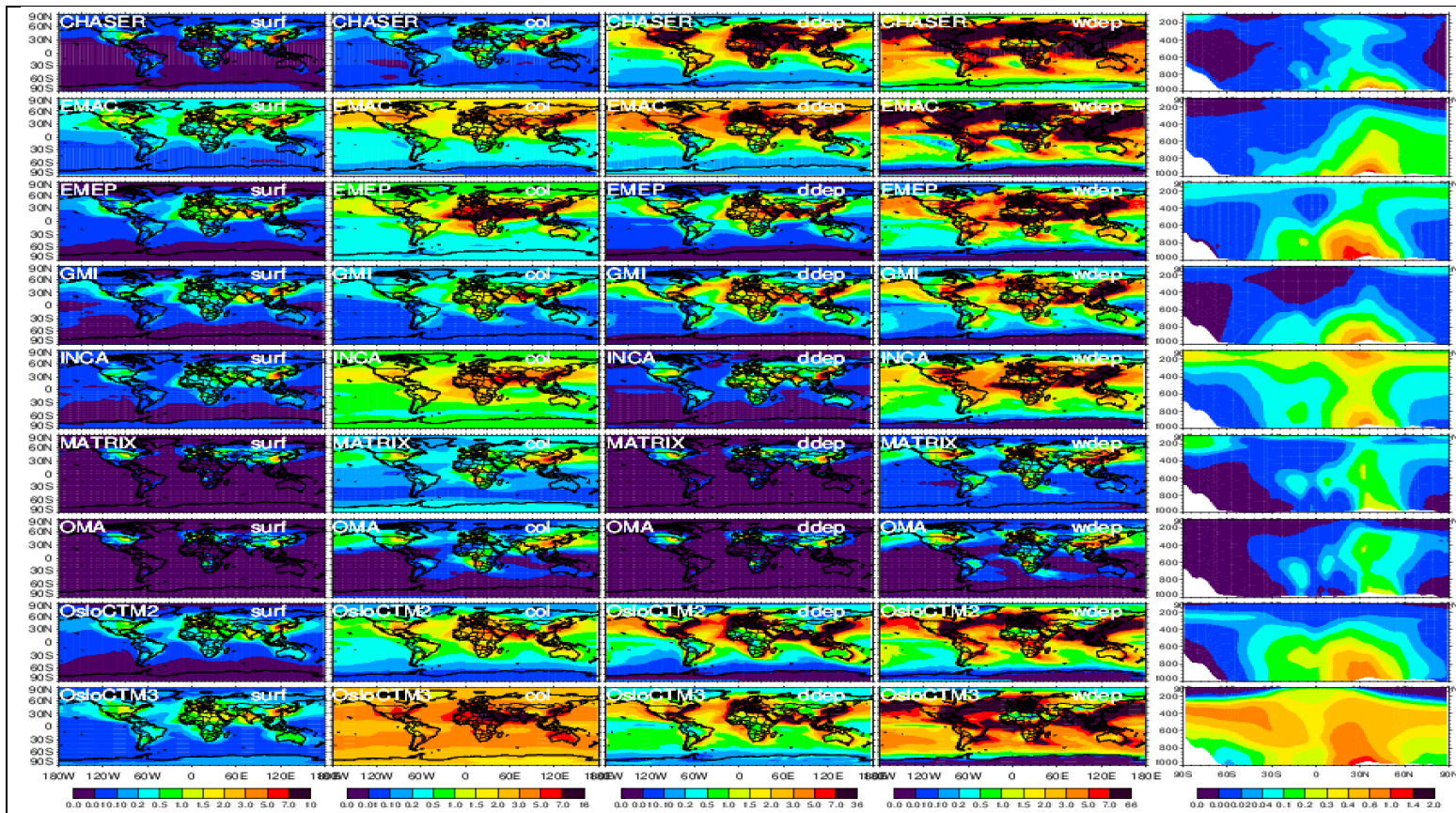


Figure 3a. Multimodel comparison of  $\text{NO}_3^-$  for surface mass mixing ratio ( $\mu\text{g kg}^{-1}$ , left), column load ( $\text{mg m}^{-2}$ , second), dry deposition ( $\text{ng m}^{-2} \text{s}^{-1}$ , third), wet deposition ( $\text{ng m}^{-2} \text{s}^{-1}$ , fourth), and vertical zonal mean ( $0.5\mu\text{g kg}^{-1}$ , right). Note that the CHASER dry and wet depositions and the EMAC wet deposition in this figure contain both  $\text{NO}_3^-$  and  $\text{HNO}_3$ , while the rest models  $\text{NO}_3^-$ .

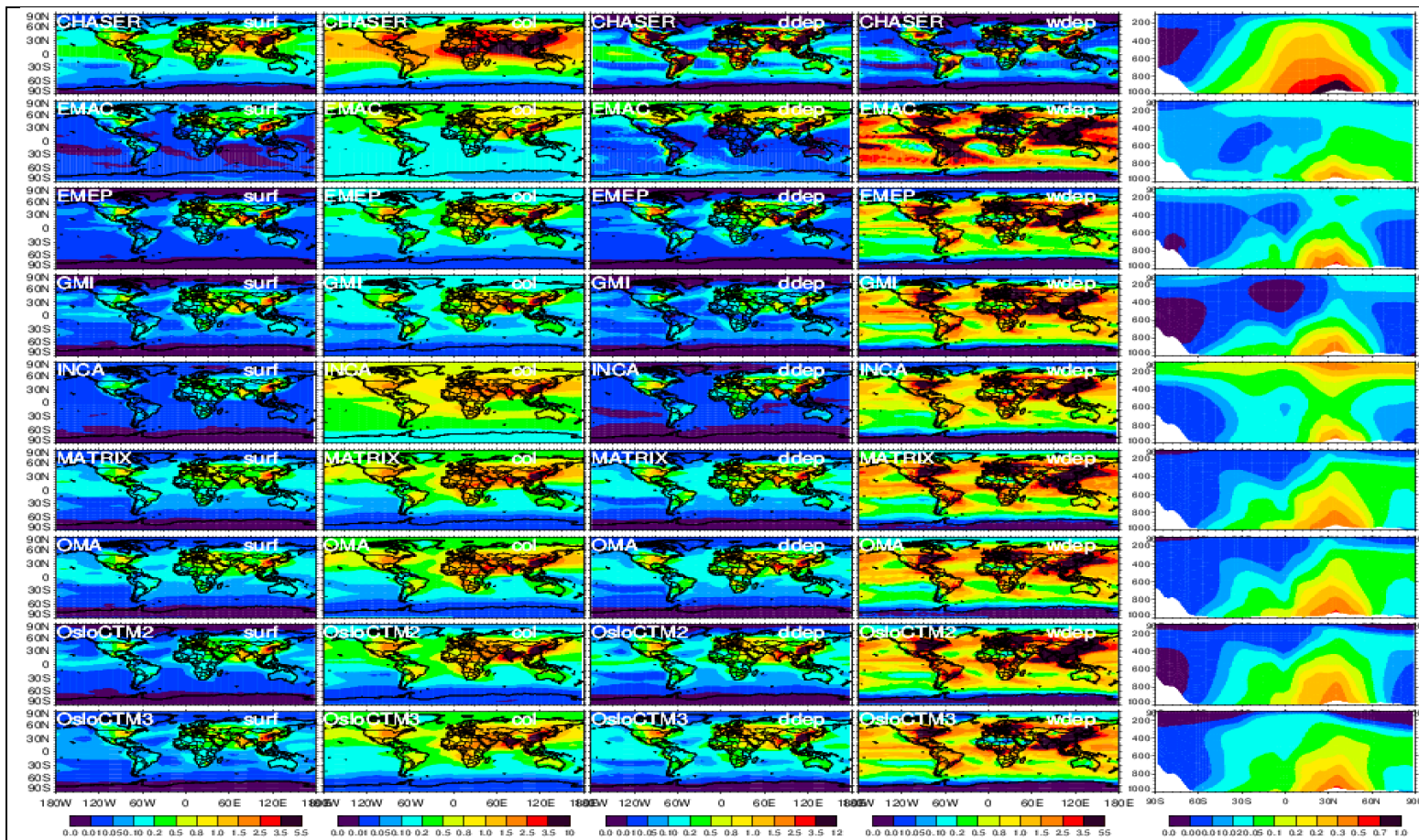


Figure 3b. Same as Figure 3a but for  $\text{NH}_4^+$  and the unit in vertical distribution is  $\mu\text{g kg}^{-1}$ . Note that the EMAC wet deposition in this figure contain both  $\text{NH}_4^+$  and  $\text{NH}_3$ , while the rest models only  $\text{NH}_4^+$ .

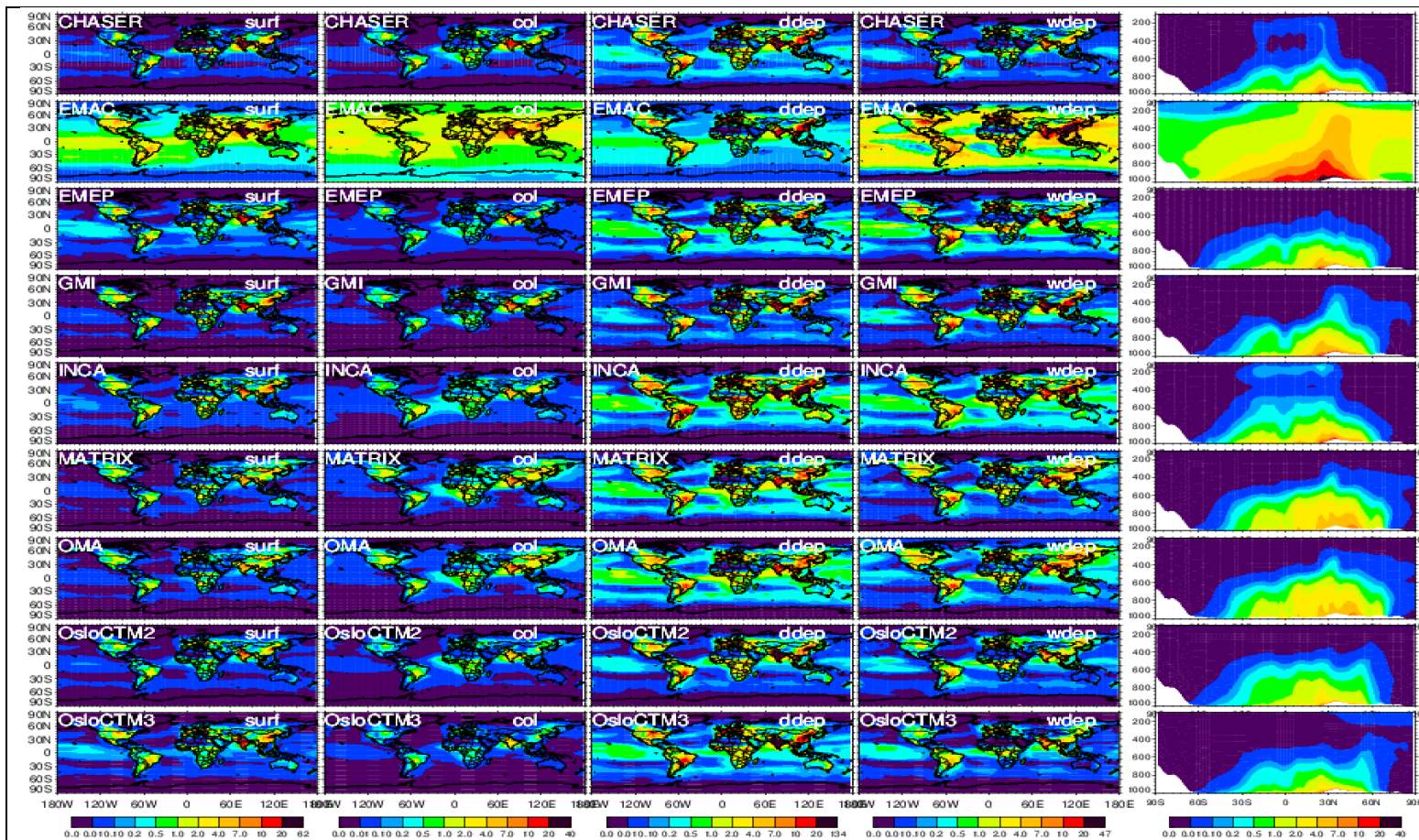


Figure 3c. Same as Figure 3a but for  $\text{NH}_3$ . Units are ppb for surface concentration and 0.1ppb for vertical distribution. Note that the EMAC wet deposition in this figure contain both  $\text{NH}_3$  and  $\text{NH}_4^+$ , while the rest models only  $\text{NH}_3$ .

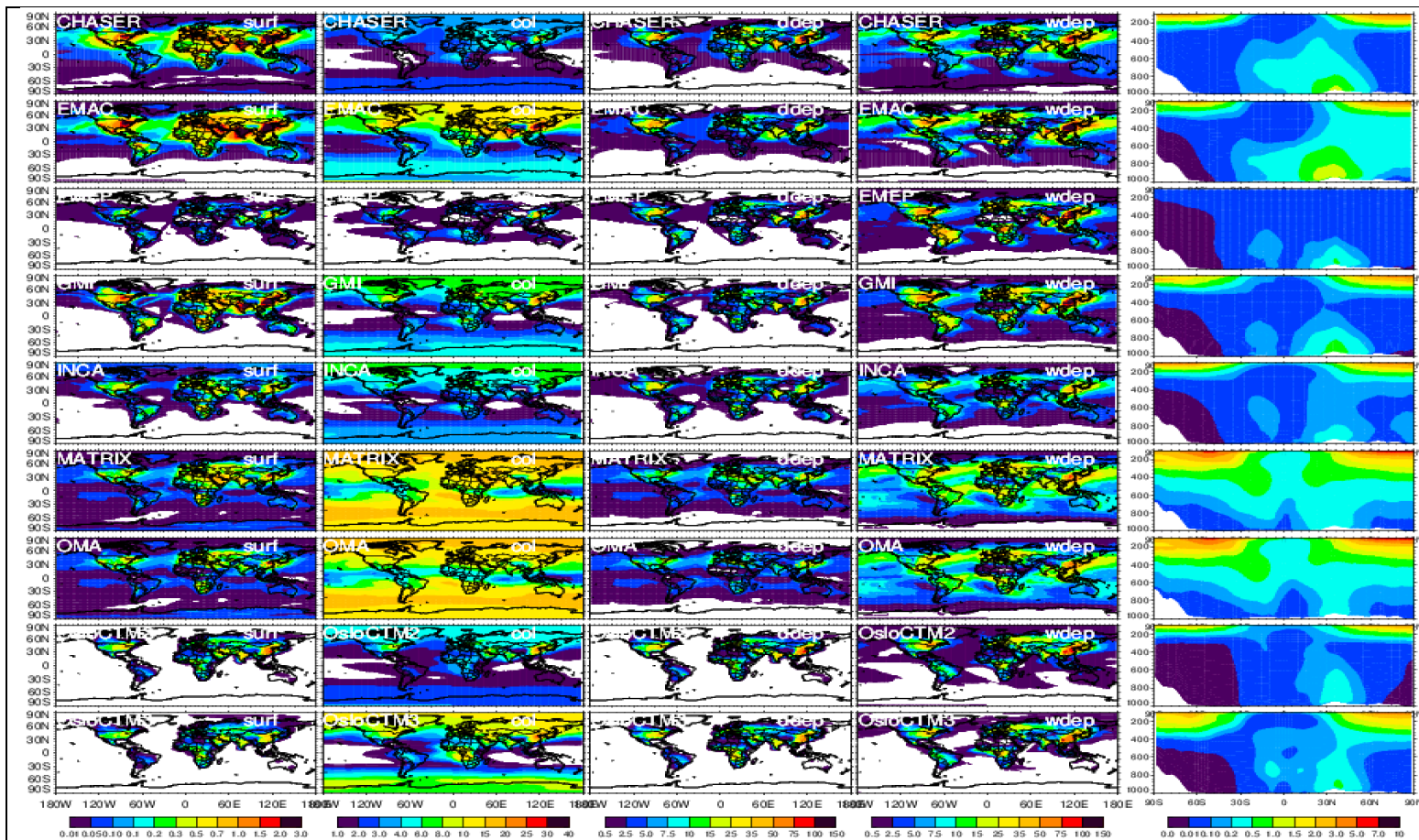


Figure 3d. Same as Figure 3a but for HNO<sub>3</sub>. Units are 100 ppb for surface concentration, mg m<sup>-2</sup> for loading, and 2ng m<sup>-2</sup> s<sup>-1</sup> for dry and wet depositions. Note that the column total of HNO<sub>3</sub> is from surface up to 100 ppb vertically. The CHASER dry and wet depositions and the EMAC wet deposition in this figure contain both HNO<sub>3</sub> and NO<sub>3</sub><sup>-</sup>, while the rest models only HNO<sub>3</sub>.

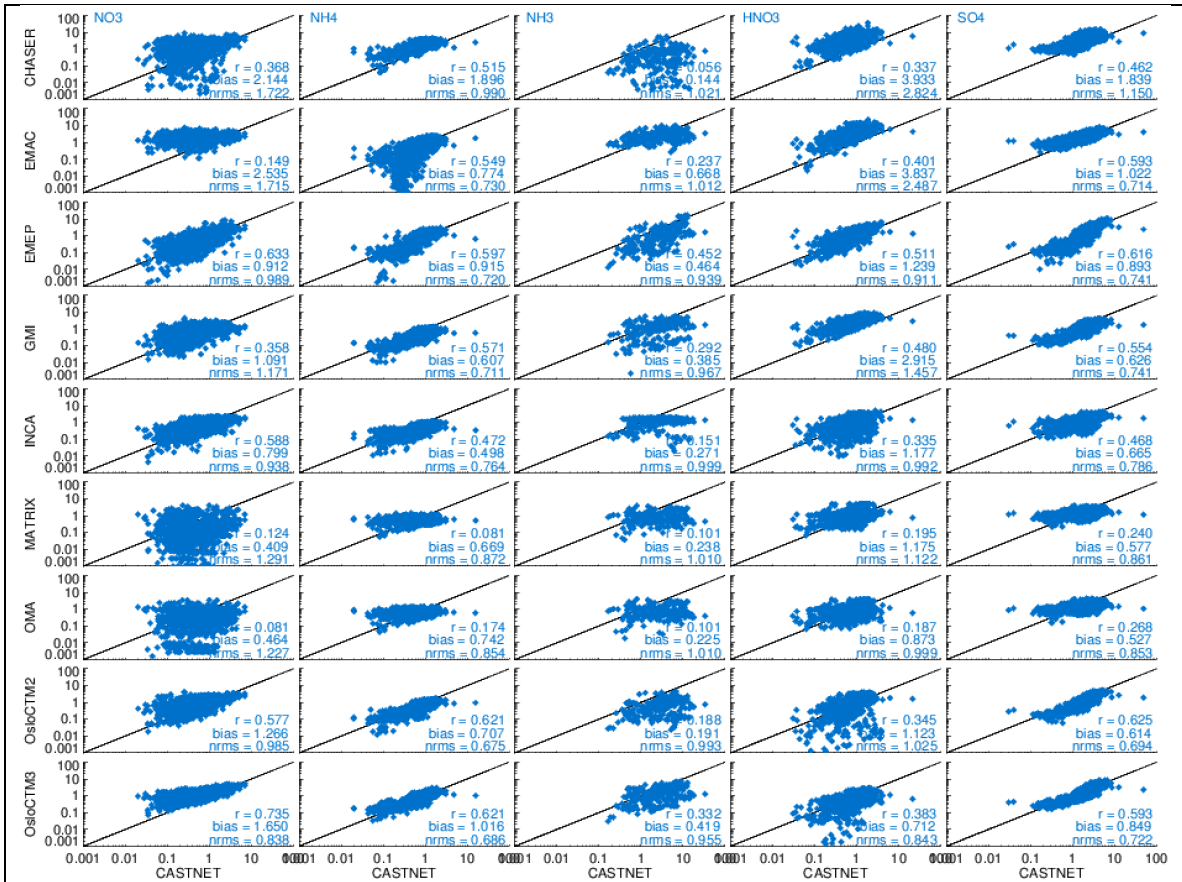


Figure 4a. Comparison of surface mixing ratios of  $\text{NO}_3^-$ ,  $\text{NH}_4^+$ ,  $\text{NH}_3$ ,  $\text{HNO}_3$ , and  $\text{SO}_4^{2-}$  between models and CASTNET measurement. Units are  $\mu\text{g m}^{-3}$ .

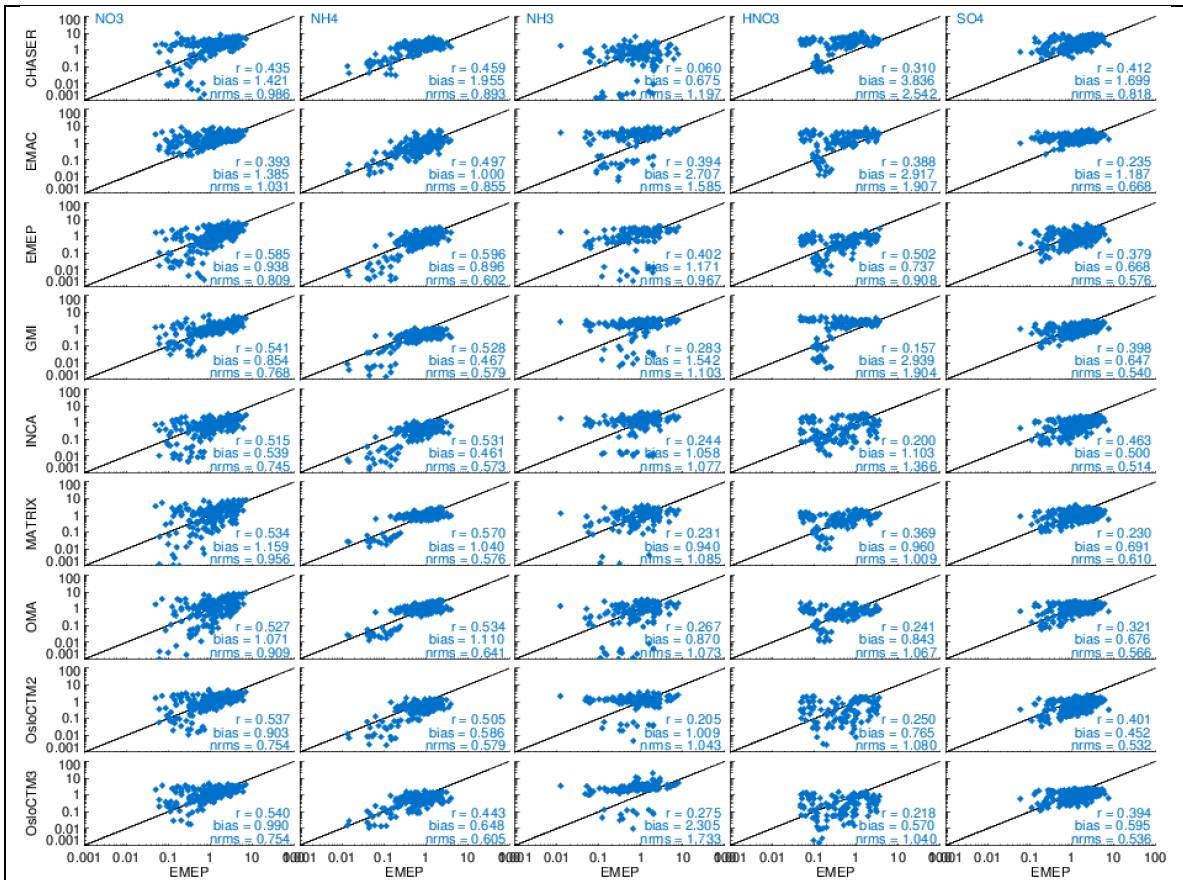


Figure 4b. Same as Figure 4a but for EMEP.

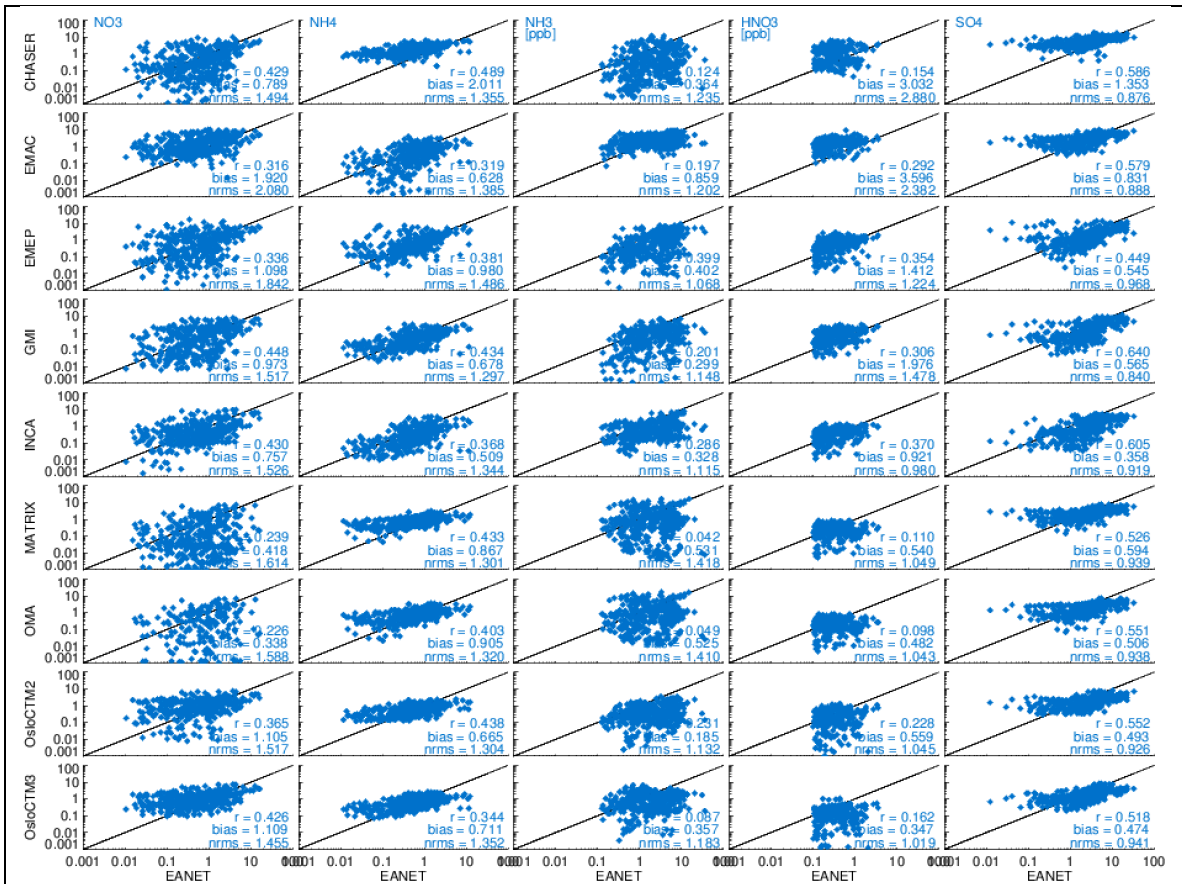


Figure 4c. Same as Figure 4a but for EANET.

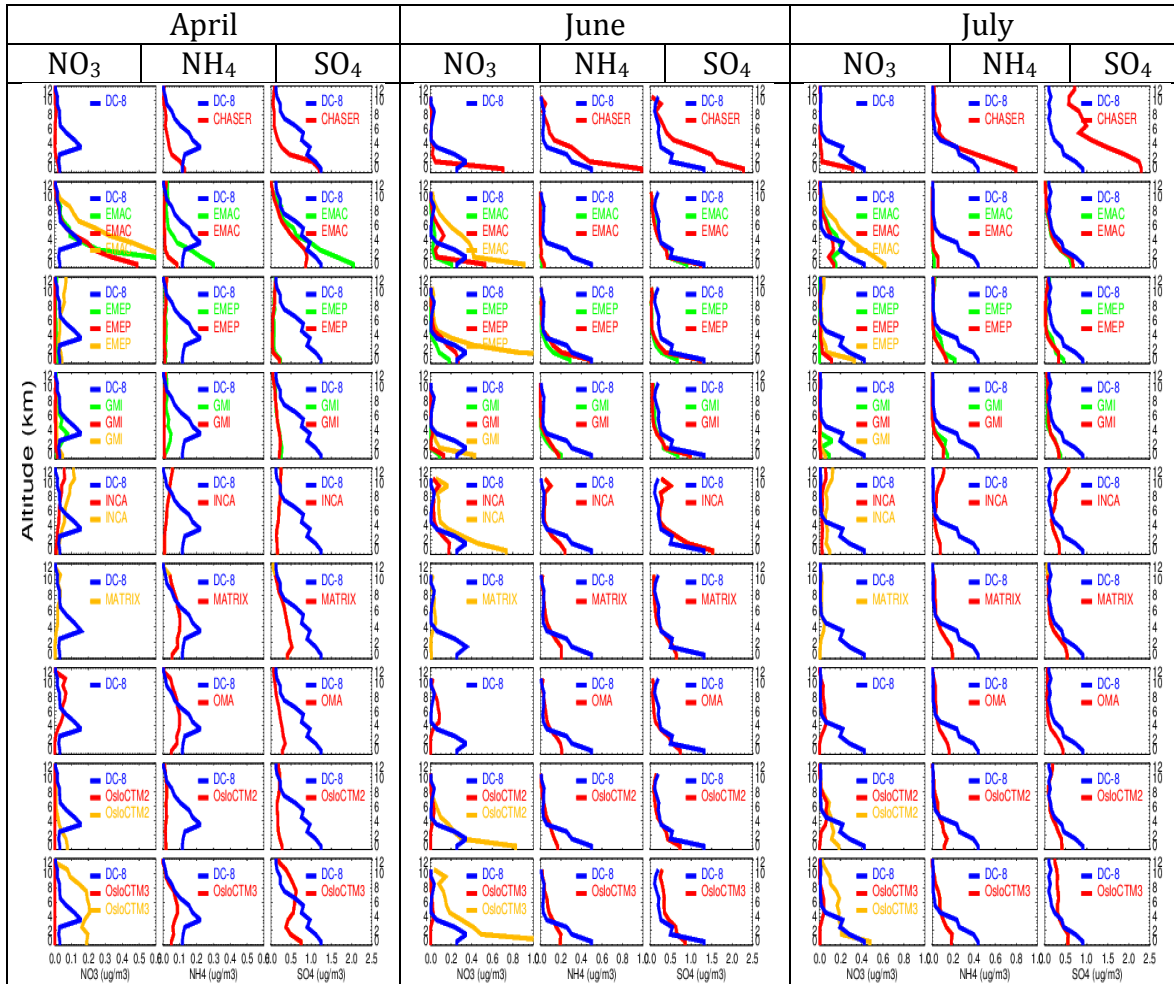


Figure 5. Vertical profile comparison between ARCTAS aircraft measurements and AeroCom model simulations. Note that ARCTAS AMS measurements give fine mode aerosols. Model profiles are shown in green (fine mode aerosol analyzed with daily output), red (fine mode aerosol with monthly output), and orange (total  $\text{NO}_3^-$  with monthly output). CHASER and OMA have fine mode  $\text{NO}_3^-$  only. Units are  $\mu\text{g m}^{-3}$ .



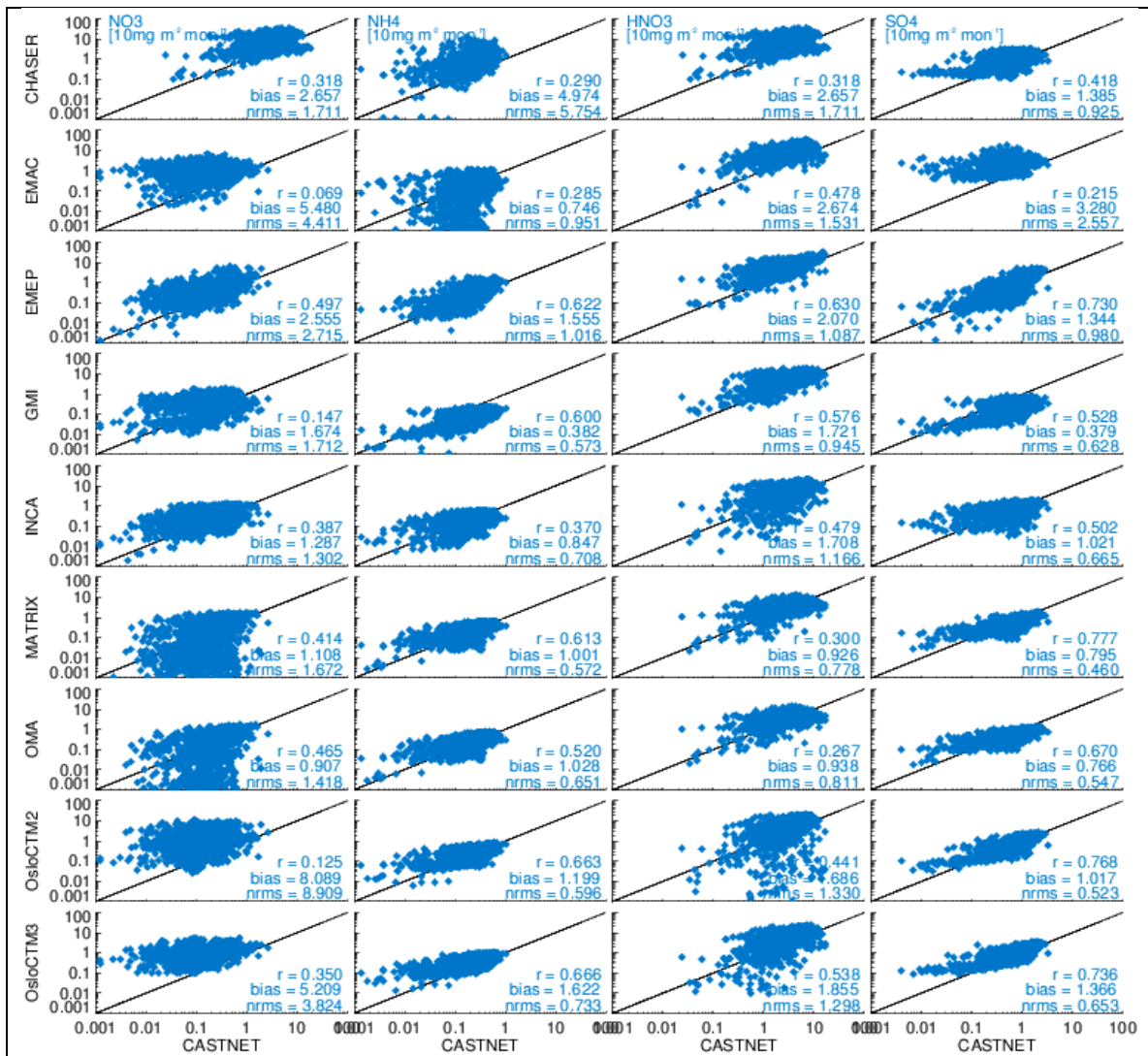


Figure 6. Comparison of surface dry deposition of  $\text{NO}_3^-$ ,  $\text{NH}_4^+$ ,  $\text{HNO}_3$ , and  $\text{SO}_4^{2-}$  between models and CASTNET measurements. Units are  $10\text{mg m}^{-2} \text{mon}^{-1}$ .

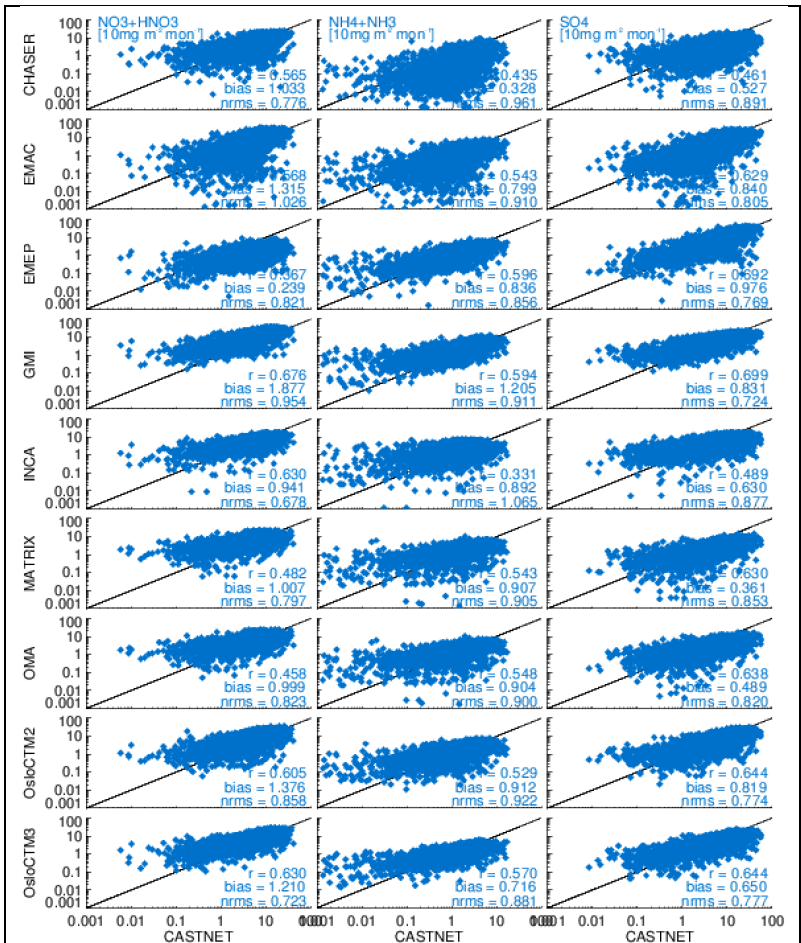


Figure 7a. Comparison of surface wet deposition of NO<sub>3</sub><sup>-</sup>+HNO<sub>3</sub>, NH<sub>4</sub><sup>+</sup>+NH<sub>3</sub>, and SO<sub>4</sub><sup>2-</sup> between models and NDAP/NTN measurements. Units are 10mg m<sup>-2</sup> mon<sup>-1</sup>.

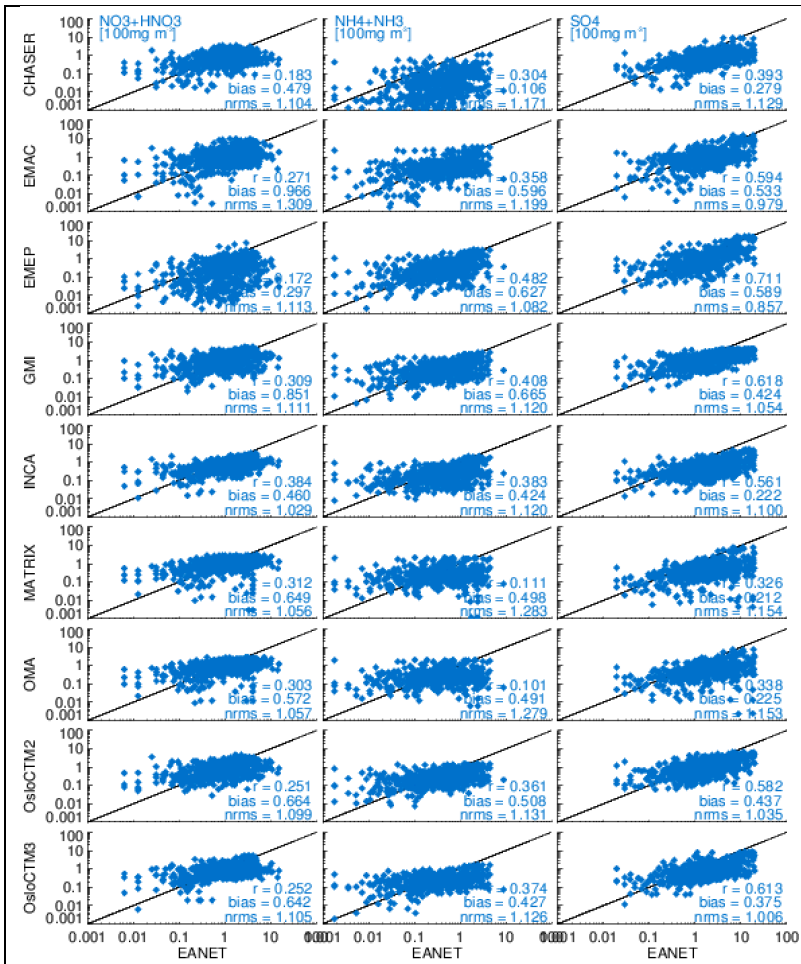


Figure 7b. Same as Figure 7a but for EANET with units of 100mg m<sup>-3</sup>.

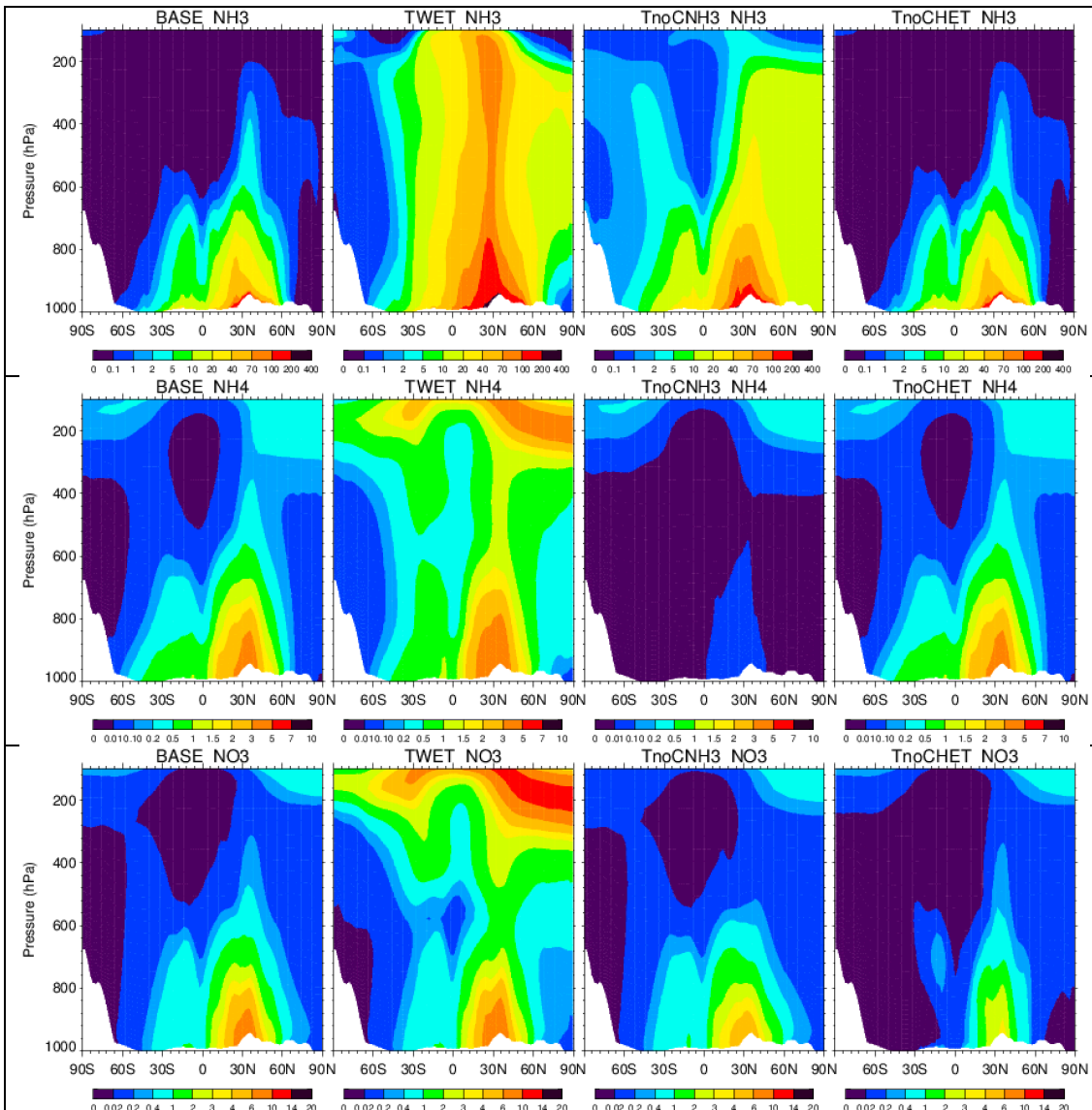


Figure 8. Zonal mean vertical distribution of  $\text{NH}_3$  (0.01 ppb),  $\text{NH}_4^+$  (0.1  $\mu\text{g kg}^{-1}$ ) and  $\text{NO}_3^-$  (0.05  $\mu\text{g kg}^{-1}$ ) from base and three sensitivity experiments explained in Table 6.

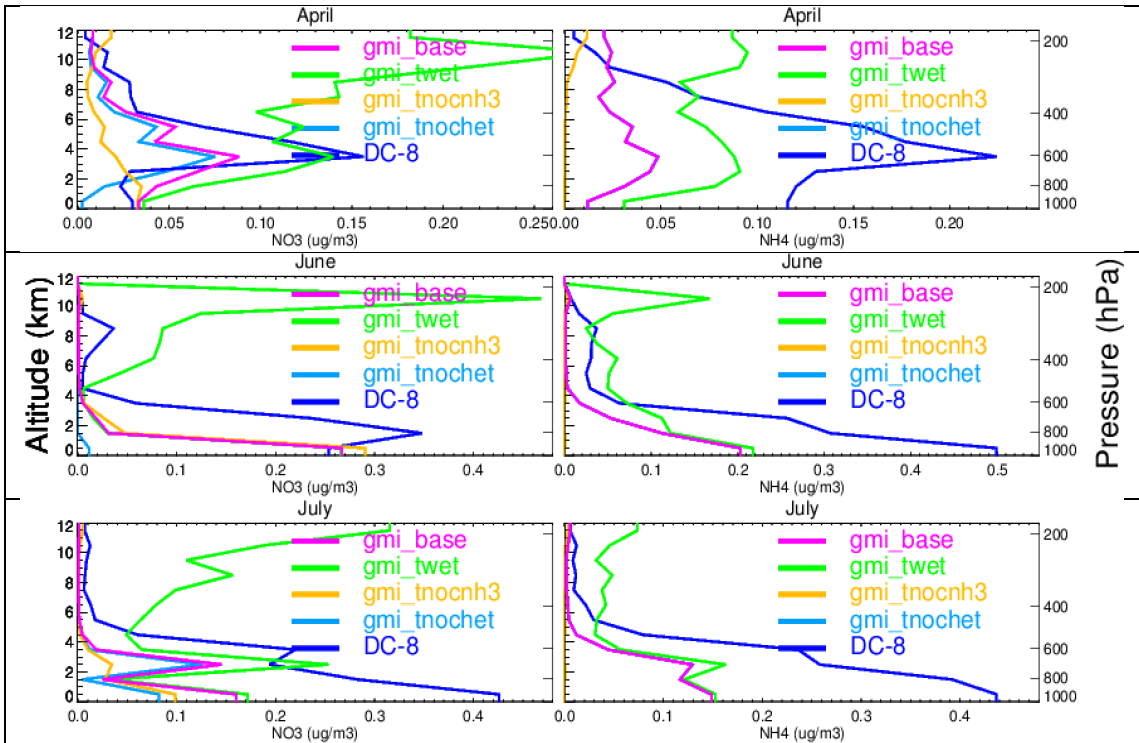


Figure 9. Comparison between GMI simulations and ARCTAS measurements of  $\text{NH}_4^+$  and  $\text{NO}_3^-$  from base and three sensitivity experiments explained in Table 6. Note the light blue line for  $[\text{NH}_4^+]$  is frequently underneath the peak line.

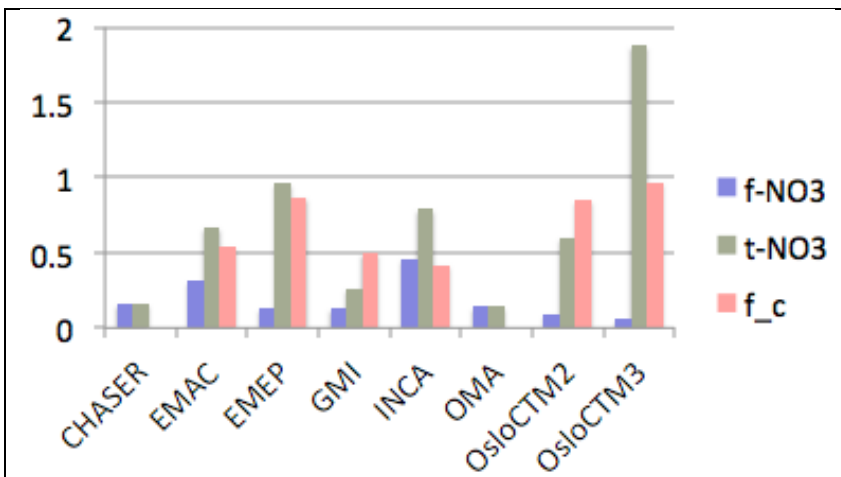


Figure 10.  $\text{NO}_3^-$  fine mode burden (f-NO3, Tg), total burden (t-NO3, Tg), and coarse mode fraction (f\_c) for the eight AeroCom models.